Karolinska Institutet

Thesis for doctoral degree (Ph.D.) 2013

The role of striatal inhibition in the processing of cortical neuronal avalanches

Andreas Klaus

Thesis for doctoral degree (Ph.D.)
2013

The role of striatal inhibition in the processing of cortical neuronal avalanches

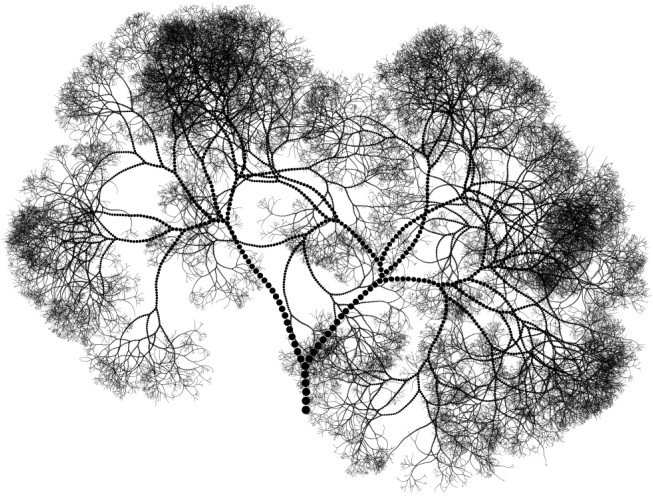

Andreas Klaus

Karolinska Institutet

From the Department of Neuroscience
Karolinska Institute, Stockholm, Sweden

The role of striatal inhibition in the processing of cortical neuronal avalanches

Andreas Klaus

Karolinska Institutet

Stockholm 2013

Published by Karolinska Institute. Printed by Larserics.

ISBN 978-91-7549-015-1

Cover art: Self-similar ("scale-invariant") object generated with Context Free (http://www.contextfreeart.org).

Mystery creates wonder, and wonder is the basis for man's desire to understand. Who knows what mysteries will be solved in our lifetime, and what new riddles will become the challenge of the new generations?

Neil Armstrong

To Martina, Susanne, and my brothers.

Summary

The brain is spontaneously active even in the absence of any obvious motor actions or sensory perceptions. This so-called resting activity or ongoing activity reflects the myriads of neuronal interactions necessary for the brain to process past actions, allow for current inputs, and prepare for future decisions and responses. In cortex, more than a decade of research has shown that resting activity exhibits a truly complex organization that partially originates from the underlying anatomy but equally important emerges from neuronal dynamics at the systems level. For the basal ganglia, despite their important role in brain function such as preparatory movement control, the organization of resting activity is barely understood. The current work centers on how the striatum, which is the main input nucleus of the basal ganglia, processes the spatiotemporally complex resting activity of the cortex.

Without a clear understanding of the spontaneous activity that arises in cortex, it would have been daunting and — most likely — impossible to approach this question experimentally. However, a decade of research has shown that spontaneous activity in cortex is precisely organized and that it is this organization that optimizes cortical networks for information processing. Spontaneous activity in superficial layers of cortex can extend over large areas with amplitude fluctuations that span multiple orders of magnitude. This activity has been identified as so-called *neuronal avalanches*, diverse spatiotemporal neuronal activity clusters that follow a power law distribution in clusters size with an exponent close to -1.5. This power law reflects balanced activity propagation where the likelihood of activity to propagate to distant cortical sites is maximized while avoiding pathological activity explosion, e.g. epilepsy. These and related measures allow for an absolute and quantitative characterization of cortical activity at rest to which striatal activity can be compared. Anatomy suggests that striatal neurons might respond to cortical neuronal avalanches and the pattern of converging and diverging corticostriatal projections suggests that neurons in the striatal microcircuit might even recombine neuronal avalanche input. The main aim of this thesis therefore was to investigate whether and how

the striatum processes fluctuating input with particular focus on cortical neuronal avalanches.

Cortical inputs, besides exciting striatal medium spiny (MS) projection neurons, which constitute about 95% of neurons in the striatum, also project to a relatively small number of local striatal interneurons, the fast-spiking (FS) neurons. FS interneurons in turn provide feedforward inhibition to MS projection neurons. The first part of this thesis on striatal processing of cortical inputs thus examined the firing patterns of FS interneurons in response to cortical inputs. Using a combination of computational modeling and *in vitro* whole-cell recordings, it is shown that input to FS neurons strongly influenced their firing pattern and spike time reliability. FS neurons fired precisely timed action potentials with little trial-to-trial variability both *in vitro* and in the model in response to fluctuating input. In contrast, FS interneurons exhibited their well-known random stuttering discharge only for constant input. Our modeling results suggest that FS firing variability, such as observed in rodents *in vivo* or in organotypic cultures *in vitro*, most likely results from input fluctuations. Importantly, this suggests that the temporal organization of cortical input to FS interneurons, as present in neuronal avalanches, translates into corresponding temporally precise feedforward inhibition of MS projection neurons. Accordingly, the short-term depression of FS-to-MS synapses further facilitated the translation of input variability at FS interneurons into variability of postsynaptic responses, i.e. feedforward inhibition, in MS projection neurons.

The deep location of the striatum in the forebrain and the sensitivity of cortical avalanches to common anesthetics currently presents huge obstacles when trying to simultaneously record cortical avalanches and striatal dynamics with cellular resolution. A major aim of this thesis therefore was to establish an experimental model system to study corticostriatal dynamics in the presence of cortical neuronal avalanches. I therefore grew organotypic cortex-striatum-substantia nigra pars compacta cultures on planar multielectrode arrays and recorded spontaneous activity simultaneously from cortical and striatal tissue. While cortical cluster sizes followed a power law distribution with an exponent close to -1.5, striatal dynamics were characterized by a power law distribution in cluster sizes with a more

negative exponent close to -3. This difference was absent under conditions of epilepsy or global disinhibition, that is, when blocking inhibition in both cortex and striatum. Thus, the significantly more negative striatal exponent under cortical avalanche conditions indeed indicates qualitatively different dynamics between cortex and striatum. In fact, the striatal local microcircuit actively decorrelates cortical neuronal avalanche input. This was demonstrated by intracellular calcium imaging of striatal neurons combined with local blockade of striatal inhibition. Under normal conditions, neuronal firing in spiny projection neurons fluctuated significantly between spatially nearby neighboring neurons and also fluctuated strongly in time between successive cortical avalanche inputs. Removal of local striatal inhibition synchronized spontaneous spiking activity between striatal neurons and increased striatal firing, overall reducing temporal fluctuations in striatal output over time. Thus, acute removal of local striatal inhibition results in a homogeneous, non-discriminatory following of striatal neurons to cortical avalanche inputs.

In conclusion, the results from this thesis suggest that the striatum pays attention to the complex spatiotemporal organization of resting activity in cortex. The locally and temporally diverse responses of striatal neurons crucially depend on the intact inhibitory striatal microcircuits. The computational results suggest that FS interneurons in principle are able to translate large fluctuations of cortical inputs into diverse and timely feedforward inhibition onto MS projection neurons, which might contribute to the active decorrelation. Alternatively, recurrent inhibition between MS projection neurons might play an important role in the striatal response to cortical resting activity. The precise contributions of these local inhibitory pathways to striatal resting activity have yet to be determined. These results clearly establish that the striatum, generally considered to be responsible for movement control, is also active during resting activity. Disturbances of the inhibitory striatal circuits might have therefore negative implications for both resting conditions and movement coordination.

List of publications

I. **Andreas Klaus**, Henrike Planert, J. J. Johannes Hjorth, Joshua D. Berke, Gilad Silberberg & Jeanette Hellgren Kotaleski (2011). Striatal fast-spiking interneurons: from firing patterns to postsynaptic impact. *Frontiers in Systems Neuroscience* 5:57.

II. Dietmar Plenz, Craig V. Stewart, Woodrow Shew, Hongdian Yang, **Andreas Klaus** & Tim Bellay (2011). Multi-electrode array recordings of neuronal avalanches in organotypic cultures. *Journal of Visualized Experiments* (54), e2949.

III. **Andreas Klaus**, Shan Yu & Dietmar Plenz (2011). Statistical analyses support power law distributions found in neuronal avalanches. *PLoS ONE* 6(5): e19779.

IV. **Andreas Klaus**[*], Shan Yu[*], Hongdian Yang & Dietmar Plenz. Cutoff in power law distributions and its implication for neuronal avalanche analyses. *Manuscript, [*]equal contribution.*

V. **Andreas Klaus** & Dietmar Plenz. Intrastriatal inhibition decorrelates cortical neuronal avalanches. *Manuscript.*

Contents

1 Introduction **1**
1.1 Basal ganglia architecture and function 1
1.2 The striatal microcircuit 2
1.2.1 Striatal afferents 2
1.2.2 Neuron types 4
1.2.3 Models of striatal information processing 7
1.3 Cortical neuronal avalanches 9

2 Aims **11**

3 Methods **13**
3.1 Neuron model of a stuttering FS interneuron 13
3.2 Synaptic input and electrical coupling in the model 14
3.3 Modeling of the FS-to-MS synaptic dynamics 15
3.4 Organotypic slice cultures 16
3.5 Multielectrode recordings 17
3.6 Local field potential and multi-unit analysis 18
3.7 Detection of spatiotemporal clusters 18
3.8 Finite-size scaling analysis 19
3.9 Statistical analyses and parameter estimation 20
3.10 Calcium imaging 23
3.11 Pharmacology 24
3.12 Immunohistochemistry and confocal imaging 26

4 Results and discussion **27**
4.1 The influence of input fluctuations on the firing patterns in FS interneurons (Paper I) 27
4.2 Organotypic cortex-striatum-substantia nigra pars compacta cultures (Paper II) 30
4.3 Statistical analyses of power law distributions in cortical neuronal avalanches (Papers III and IV) 32
4.4 Intrastriatal inhibition decorrelates cortical neuronal avalanches (Paper V) 37

5 Conclusions and future perspectives **43**

Acknowledgments **45**

References **47**

List of abbreviations

ACSF	artificial cerebrospinal fluid
AMPA	α-amino-3-hydroxyl-5-methyl-4-isoxazole-propionate
AP	action potential
Ctx	cortex
DIV	day *in vitro*
FS	fast-spiking
GABA	γ-aminobutyric acid
GPi/e	internal/external segment of the globus pallidus
HBSS	Hank's buffered saline solution
KS	Kolmogorov-Smirnov
LFP	local field potential
LLR	log-likelihood ratio
MEA	multi-/microelectrode array
MS	medium spiny
MU	multi-unit
nLFP	negative local field potential
NMDA	N-methyl-D-aspartate
NPY	neuropeptide Y
OGB	Oregon Green 488 BAPTA-1
PDF	probability density function
(P)LTS	(plateau depolarization and) low-threshold spike
PMF	probability mass function
PSP	postsynaptic potential
PTX	picrotoxin
SD	standard deviation
SNc/r	substantia nigra pars compacta/reticulata
SR101	sulforhodamine 101
STN	subthalamic nucleus
Str	striatum
TH	tyrosine hydroxylase
VTA	ventral tegmental area

1 Introduction

1.1 Basal ganglia architecture and function

The cortico-basal ganglia-thalamic network is involved in the motivational and habitual control of cognitive and motor functions (Albin et al., 1989; Redgrave et al., 2010; Yin and Knowlton, 2006). The contribution of the basal ganglia to these functions is apparent from the broad spectrum of cognitive and movement disorders that are caused by dysfunctions of these nuclei (Denny-Brown, 1962; Wichmann and DeLong, 1996; Graybiel, 2008). The basal ganglia integrate excitatory, glutamatergic input from the cortex and thalamus in functionally segregated pathways (McGeorge and Faull, 1989; Bolam et al., 2000; Smith et al., 2004), and exert GABA-mediated inhibition over brainstem targets and the thalamocortical network (DeLong and Wichmann, 2009). The striatum, the major input nucleus of the basal ganglia, sends direct GABAergic projections to the output nuclei, that is, the internal segment of the globus pallidus (GPi) and the substantia nigra pars reticulata (SNr) (Féger and Crossman, 1984; Alexander and Crutcher, 1990). This so-called *direct* pathway is complemented by the *indirect* pathway, which sends striatal output to the GPi and SNr via the external segment of the globus pallidus (GPe) and the subthalamic nucleus (STN).

The basal ganglia output neurons in the GPi and SNr are tonically active, thus exerting a certain tonic inhibition onto thalamocortical (and brainstem) targets. The two pathways are considered to have largely opposite downstream effects, that is, the direct pathway facilitates thalamocortical network activity (Deniau and Chevalier, 1985), whereas the indirect pathway imposes inhibition. The balance between the two pathways critically depends on the dopaminergic input from the substantia nigra pars compacta (SNc). Striatofugal neurons of the direct pathway express dopamine D1 receptors, whereas indirect pathway neurons express predominantly dopamine D2 receptors (Gerfen et al., 1990; Bertran-Gonzalez et al., 2010). Degeneration of dopaminergic neurons of the SNc eventually leads to increased synchronized burst activity in the GPe, STN and GPi/SNr (Bergman et al., 1998; Plenz and Kital, 1999; Brown et al., 2001; Hammond et al., 2007; DeLong and Wichmann, 2009; Cruz et al., 2009). This type of abnormal activity strongly correlates with the devastating motor impairments found in Parkin-

son's disease. Drug therapy (e.g., levodopa or apomorphine) and/or deep brain stimulation of the STN, GPi or related nuclei (Bergman et al., 1990; Marsden and Obeso, 1994; Clarke et al., 2009) reduces abnormal bursting and ameliorates neurological dysfunctions. In addition to the two pathways described above, a third major pathway has been identified that does not involve the striatum. The so-called *hyperdirect* pathway links the cortex directly to the STN, which excites the GPi/SNr via its glutamatergic projection (Bolam et al., 2000; Nambu, 2008). This pathway appears to be important for normal basal ganglia function (Aron and Poldrack, 2006; Gradinaru et al., 2009; Redgrave et al., 2010), and is also involved in some of the impairments observed in Parkinson's disease, such as tremor (Leblois et al., 2006; Redgrave et al., 2010).

This brief description of the major anatomical structures of the basal ganglia and their linkages with cortex and other forebrain and midbrain structures already outlines the enormous functional complexity faced when trying to understand the basal ganglia network under normal and pathological conditions (Marsden and Obeso, 1994; DeLong and Wichmann, 2009; Redgrave et al., 2010). Additional complexity is given, for example, by the extensive feedback loops within the basal ganglia (e.g., Mallet et al., 2012) and by the axon collaterals that distribute neuronal activity more broadly than considered in most models (Parent et al., 2000). In addition, the anatomical description of the basal ganglia largely neglects the dynamics of the input that the basal ganglia receive as well as the processing that is performed within each nucleus (Bar-Gad et al., 2003). In the current thesis, this aspect was studied in detail for the corticostriatal system as will be described below.

1.2 The striatal microcircuit

1.2.1 Striatal afferents

The striatum is the largest nucleus of the basal ganglia and the major input stage. At a large scale, the projection from the cortex to the striatum is topographically organized (Kemp and Powell, 1970; McGeorge and Faull, 1989; Kincaid et al., 1998). Yet, as tracing methods improved, a complex picture emerged with cortical areas that are reciprocally connected

in cortex revealing overlapping target regions in the striatum (Gerfen and Sawchenko, 1984; Gerfen, 1989; Selemon and Goldman-Rakic, 1985; Flaherty and Graybiel, 1994; Parent and Hazrati, 1995; McFarland and Haber, 2000; Haber and Calzavara, 2009). Small areas within the cortex often span multiple projection zones in the striatum, providing essential building blocks for combinatorial evaluation of input from different cortical areas at the striatal level (Kincaid et al., 1998; Zheng and Wilson, 2002). Despite the general topographical organization, corticostriatal projections show also convergence from motor and somatosensory areas, and multisensory integration (Ramanathan et al., 2002; Reig and Silberberg, 2012). A similar complex organization has been reported for the thalamostriatal projections (Powell and Cowan, 1956; Jones and Leavitt, 1974; Berendse and Groenewegen, 1990; Smith et al., 2004, 2009). Both cortico- and thalamostriatal synapses use glutamate as their neurotransmitter and together they account for the majority of striatal synapses (Wilson, 2007). *In vitro*, thalamostriatal synapses have a higher release probability than corticostriatal synapses and show short-term synaptic depression with repetitive stimulation (Ding et al., 2008). This suggests that functionally, a single spike or short burst from a thalamostriatal projection neuron can have a strong functional impact. In contrast, corticostriatal synapses show short-term synaptic facilitation in response to short, repeated stimulation (Mahon et al., 2000; Ding et al., 2008) and exhibit various forms of long-term synaptic changes (Di Filippo et al., 2009; Gerfen and Surmeier, 2011). This suggests that a corticostriatal projection neuron might increase its impact on striatal projection neurons through prolonged burst activity. The striatum has the highest density of dopaminergic synapses arising from the midbrain SNc. Not surprisingly, dopamine plays a significant role in long-term plasticity of corticostriatal synapses, which converge with dopaminergic terminals on the dendrites of striatal projection neurons (Reynolds et al., 2001; Smith et al., 2004; Calabresi et al., 2007; Tritsch and Sabatini, 2012). Besides glutamatergic input from cortex and thalamus, the striatum receives considerable GABAergic input from the external segment of the globus pallidus (Bevan et al., 1998; Mallet et al., 2012) as well as neuromodulatory serotonergic input from the dorsal raphe nucleus (Soubrié et al., 1984).

1.2.2 Neuron types

Medium spiny projection neurons

The medium-sized spiny (MS) projection neuron constitutes the majority of neurons in the striatum. For example, in rodents, they are estimated to make up more than 95% of all striatal neurons (Oorschot, 1996). MS neurons are divided into two groups based on their projection targets, which largely correlates with the expression of specific dopamine receptors. The first group expresses dopamine D1 receptors and forms the direct pathway; whereas the second group, which expresses predominantly dopamine D2 receptors, gives rise to the indirect pathway (see above).

MS neurons are characterized by a low firing rate *in vitro* and *in vivo* (Plenz and Kitai, 1998a; Berke, 2008). Under anesthesia and in organotypic cultures, MS neurons show spontaneous transitions from a hyperpolarized resting potential (i.e., the *down-state*) to a depolarized membrane potential (i.e, the *up-state*) close to spiking threshold (Wilson and Kawaguchi, 1996; Stern et al., 1997; Plenz and Kitai, 1998a; Kerr and Plenz, 2004). The hyperpolarized resting potential is the result of an inward-rectifying potassium current (Calabresi et al., 1987; Nisenbaum and Wilson, 1995). This conductance inactivates at more depolarized membrane potentials and requires the neuron to receive sufficient input in order to enter the up-state (Wilson and Kawaguchi, 1996).

It has been consistently shown that the excitatory drive MS neurons experience during an up-state is accompanied by strong inhibitory input (Wilson and Kawaguchi, 1996; Blackwell et al., 2003; Wilson, 2009). However, the precise source of this inhibition has been, and still is, highly controversial. MS cells provide lateral connections onto the dendritic regions of neighboring MS neurons (Wilson and Groves, 1980; Bolam et al., 2000; Wilson, 2007). These anatomically well described MS-to-MS connections, initially, had been difficult to identify physiologically (Jaeger et al., 1994; but see Park et al., 1980; Katayama et al., 1981; Guzmán et al., 2003). Since then, pairwise recordings in acute slices and organotypic cultures using numerous different techniques that also include whole-cell patch recordings, and/or visual control of identifying nearby MS neurons, and reasonably high numbers of recordings to increase the likelihood of finding connected pairs of

MS neurons, clearly established that MS neurons communicate with each other through $GABA_A$-synapses (Tunstall et al., 2002; Czubayko and Plenz, 2002; Gustafson et al., 2006; Tecuapetla et al., 2007; Planert et al., 2010; Gittis et al., 2010). Since then, one of the most debated topics in striatal physiology has been the functional role of these connections. Surely, due to the fact that the chloride reversal potential in MS neurons is located between resting potential and spike threshold, MS-to-MS input, by interacting with intrinsic conductances as well as excitatory inputs, might act in numerous ways to modulate action potential firing in these neurons. However, the direct effect of MS-to-MS inputs on action potential firing has been difficult to establish (see, e.g., Gustafson et al., 2006), and it is currently not clear how the lateral interaction between MS neurons compares functionally with GABAergic input provided by striatal interneurons. A network of lateral inhibition between individual MS neurons or groups of MS cells could provide a framework to decorrelate or select among alternatives (e.g., alternative motor programs) represented in the cortical input, as hypothesized in some models of striatal function (see below). In a recent study it has been shown that the lateral connections among MS neurons are disturbed in Parkinson's disease (Taverna et al., 2008), although it is not clear whether and to what extent this contributes to changes in the neuronal activity of the basal ganglia.

Parvalbumin-expressing fast-spiking interneurons

Striatal parvalbumin-positive fast-spiking (FS) interneurons constitute ∼1% of striatal neurons (Kita et al., 1990; Luk and Sadikot, 2001). They are characterized by a high spontaneous firing rate *in vitro* and *in vivo* (Plenz and Kitai, 1998a; Berke et al., 2004). FS neurons provide proximal, GABAergic input in a highly selective manner to MS neurons (Koós and Tepper, 1999; Tepper et al., 2004; Szydlowski et al., 2013) with synapses that show short-term synaptic depression (Plenz and Kitai, 1998a; Koós et al., 2004; Gustafson et al., 2006; Planert et al., 2010; Gittis et al., 2010). Such synaptic dynamics lowers the synaptic efficacy during repeated firing. Together with the lack of synchronized activity among FS interneurons *in vivo* (Berke, 2008), it raises the question of the ultimate impact FS neurons have over MS firing. In line with a selective functional role of the feedforward inhibi-

tion provided by FS neurons onto striatal output, both FS and MS neurons showed an opposite direction selectivity in a left/right movement choice task (Gage et al., 2010). However, amphetamine treatment, which increases FS firing and motor activity, has no consistent effect on changes in MS spiking (Wiltschko et al., 2010). If FS firing changes can affect motor behavior, it is expected to be mediated in one way or another by the MS projection neurons. The effect of FS neurons on motor output is supported further by a study, in which the pharmacological blockade of AMPA-mediated input to FS neurons resulted in dyskinesia (Gittis et al., 2010), although the involvement of other interneurons cannot be completely ruled out.

Neuropeptide Y-expressing interneurons

These cells, which make up less than 1% of all striatal neurons, express the neuropeptide Y (NPY; Kawaguchi et al., 1995; Ibáñez Sandoval et al., 2011). They can be further divided depending on their electrophysiological and immunohistochemical properties. One group of NPY-expressing cells co-expresses somatostatin and nitric oxide synthase and shows low plateau depolarization and low-threshold spikes (PLTS) in response to current injections (Kawaguchi, 1993; Ibáñez Sandoval et al., 2011). A distinct group, the NPY-neurogliaform interneuron, lacks somatostatin and nitric oxide synthase staining and does not exhibit the PLTS properties of the first group (Ibáñez Sandoval et al., 2011). In contrast to the NPY-PLTS interneurons, NPY-neurogliaform cells have been shown to innervate MS neurons. This inhibitory circuit can be activated by cholinergic interneurons and suppresses firing in MS output neurons (English et al., 2012).

Cholinergic interneurons

Striatal acetylcholine-releasing interneurons, which are identified by their immunoreactivity for choline acetyltransferase, comprise a similar small fraction of striatal neurons than the above classes of interneurons (Kawaguchi et al., 1995; Raz et al., 1996; Goldberg and Wilson, 2010) and receive glutamatergic input mainly from the thalamus (Lapper and Bolam, 1992). These neurons possess large cell bodies (50–60 μm in length) and exhibit tonic firing (Wilson et al., 1990; Goldberg and Wilson, 2010). The neurotransmitter acetylcholine regulates the release of dopamine and increases FS

cell excitability via nicotinic receptors (Zhou et al., 2001; Koós and Tepper, 2002; Goldberg and Reynolds, 2011), reduces glutamatergic and GABAergic transmission in MS neurons via presynaptic muscarinic receptors (Koós and Tepper, 2002; Perez-Rosello et al., 2005; Goldberg and Reynolds, 2011), and modulates long-term synaptic changes of corticostriatal synapses (Lovinger, 2010).

In vivo, striatal cholinergic neurons change their activity in concert with nigral dopaminergic cells (Morris et al., 2004; Goldberg and Reynolds, 2011). While the dopaminergic neurons encode reward prediction error (mainly increasing dopamine release in response to rewarding stimuli), cholinergic neurons respond with an invariant firing pause to reward-related events (Morris et al., 2004) and a subsequent increase in firing (Joshua et al., 2008). In a recent study, this excitation has been shown to strongly engage NPY-neurogliaform interneurons via nicotinic receptors, which in turn provide significant inhibition onto MS neurons (English et al., 2012). Thus, striatal cholinergic neurons have not only a modulatory or long-term influence on the striatal microcircuit, but can control striatal output via GABAergic interneurons. Because the firing discharge of cholinergic interneurons *in vivo* is considerably synchronized and the rate changes occur well-timed (Raz et al., 1996; Morris et al., 2004), the drive provided to the NPY-neurogliaform cells is expected to be rather stereotypical.

Other interneurons

The striatum contains a small fraction of other interneurons, which have not been studied to the same extent as the cell types mentioned above. Among those are the calretinin-expressing, GABA-releasing interneurons (Kawaguchi et al., 1995), and striatal tyrosine hydroxylase-positive cells (Tepper et al., 2010).

1.2.3 Models of striatal information processing

A single striatal MS neuron receives input from more than 5000 cortical neurons, each of which makes only a single or at maximum a few synaptic contacts predominantly onto dendritic spines (Kincaid et al., 1998; Wilson, 2007). From the perspective of the MS neuron, this represents a massive

convergence of cortical input and is interesting from a computational perspective. Initially shown for multilayer feedforward networks (Hornik et al., 1989), also single layer networks are able to approximate any continuous function (Auer et al., 2008). The function of the corticostriatal connectivity has been explored in the context of generalization in some striatal models (Dominey et al., 1995; Plenz and Kitai, 2000). Most computational network studies of the striatum, though, focused on the lateral connections between the MS projection neurons (Wickens et al., 1991; Wickens and Oorschot, 2000; Ponzi and Wickens, 2010) and the influence of inhibitory interneurons (Wickens and Arbuthnott, 1993; Humphries et al., 2009). Early models of lateral competitive inhibition among MS neurons investigated the so-called *winner-takes-all* dynamics, that is, a scheme in which the synaptic connections of a neuron are strong enough to inhibit all its neighbors and to dominate striatal output (Wickens and Oorschot, 2000; Plenz and Kitai, 2000). Because MS collaterals were found to be electrophysiologically less strong than originally expected (Tepper et al., 2004), recent modeling studies consider network effects in which lateral inhibition can form correlated and anticorrelated cell assemblies (Humphries et al., 2009; Ponzi and Wickens, 2010). These models show temporal switching of activity, a feature that has also been observed in early striatal models (Gillies and Arbuthnott, 2000). Because the switching dynamics does not require changing input, the striatum might have the required circuitry for the sequencing of actions as suggested from experimental studies (Kermadi and Joseph, 1995; Aldridge and Berridge, 1998). Temporal switching of cell groups in sparse, asymmetrically connected inhibitory networks has also been modeled in the olfactory system, where it can produce a rich, input-specific temporal structure of output neurons (Rabinovich et al., 2000). The dynamical behavior of these models is interesting because temporal profiles that resemble the switching of cells or cell assemblies have also been observed experimentally *in vitro* and *in vivo* (Carrillo-Reid et al., 2008; Miller et al., 2008; Berke, 2008).

Lateral competitive networks are often associated with the notion of "action selection," in which some activity is gated through the striatum whereas alternative activities are filtered out. A different idea, which does not assume loss of information, is the reinforcement-driven dimensionality reduc-

tion (Bar-Gad et al., 2000, 2003). In this model, corticostriatal and lateral connections form a low-dimensional representation of the cortical activity. Interestingly, lateral connections are only needed during the (reinforcement-driven) learning phase and become weak after a representation of the input statistics has been modeled by the plastic corticostriatal synapses (Bar-Gad et al., 2000; Plenz and Kitai, 2000; Plenz, 2003).

1.3 Cortical neuronal avalanches

An interesting property of cortical networks is their ability to spontaneously generate diverse activity patterns (Fox and Raichle, 2007; Harris and Thiele, 2011) that can engage large parts of the network and span a wide range of amplitudes (Smith and Kohn, 2008; Ringach, 2009; Plenz, 2012). Several studies have shown that these activities in large part determine the high variability of evoked cortical responses, that is, a deterministic evoked component is linearly superimposed on "random" spontaneous activity resulting in variable trial-to-trial responses (Arieli et al., 1996; Fox et al., 2005).

Despite its large spatiotemporal diversity, clusters of negative local field deflections measured with multielectrode arrays in superficial cortical layers have recently been shown to follow precise statistical laws (Beggs and Plenz, 2003; Klaus et al., 2011; Yu et al., 2011; Plenz, 2012). These activity clusters, so-called *neuronal avalanches*, can be described by a scale-free power law distribution $P(s) \propto s^{\alpha}$ with an exponent α close to -1.5, where $P(s)$ denotes the probability of a neuronal avalanche of size s (Beggs and Plenz, 2003). A power law with particular exponent -1.5 is indicative of long-range correlations (Jensen, 1998) as a result of balanced activity propagation, in which one active site in the network on average triggers another active site in the near future (Plenz, 2012). Consequently, pharmacological manipulations that disturb excitatory or inhibitory synaptic transmission also abolish the power law scaling (Beggs and Plenz, 2003; Plenz, 2012). These observations are in line with critical state dynamics in the cortex and led to theoretical predictions of optimal properties in critical networks (Beggs and Plenz, 2003; Kinouchi and Copelli, 2006; Tanaka et al., 2008). In subsequent studies it has been shown that cortical networks that exhibit neuronal avalanches have a maximum dynamic range, coding capacity, and phase variability (Shew et al., 2009, 2011; Yang et al., 2012), all features that may support information processing and storage.

Neuronal avalanches have been identified in the local field activity *in vitro* in organotypic cultures and acute slices (Beggs and Plenz, 2003; Stewart and Plenz, 2006), *in vivo* in anesthetized rats and awake monkeys (Gireesh and Plenz, 2008; Petermann et al., 2009; Yu et al., 2011), in spiking activity *in vitro* and *in vivo* (Pasquale et al., 2008; Hahn et al., 2010; Ribeiro et al., 2010), and in the blood-oxygen-level-dependent and magnetoencephalographic signal in humans (Tagliazucchi et al., 2012; Shriki et al., under revision). Changes in these dynamics have been observed after pharmacological manipulations of synaptic transmission (Beggs and Plenz, 2003; Shew et al., 2009) and in recordings of epileptic tissue (Hobbs et al., 2010; Meisel et al., 2012). Thus, the scale-free dynamics in neuronal avalanches that are characterized by a power law with exponent -1.5 represent an absolute reference point from which deviations from normal resting activity can be precisely quantified (Shew et al., 2009; Meisel et al., 2012; Plenz, 2012).

As described in the previous sections, striatal neurons require spatiotemporal correlations in the cortical input to enter the up-state during which they fire action potentials. The wide range of amplitudes and levels of phase synchronization during neuronal avalanches (Beggs and Plenz, 2003; Yang et al., 2012), however, raises the question whether the striatum is exposed to the scale-free cortical activity given the low firing rate in striatal MS neurons under normal conditions (Plenz and Kitai, 1998a; Berke et al., 2004).

2 Aims

The striatum is the main input nucleus of the basal ganglia, a set of subcortical nuclei that are involved in normal and abnormal brain function. The research presented in the current thesis is concerned with the mechanisms that underlie the corticostriatal network dynamics under spontaneous (i.e., resting) conditions, and their proper statistical description.

The main objectives of the present thesis were:

- To identify the essential factors that control firing patterns in striatal fast-spiking interneurons (Paper I).
- To establish an *in vitro* model in which striatal processing of cortical neuronal avalanches can be studied experimentally (Paper II).
- To establish stringent statistical analyses to test for the presence of cortical neuronal avalanches (Papers III and IV).
- To study whether and how the striatum processes cortical neuronal avalanches (Paper V).

3 Methods

All animal procedures were in accordance with guidelines of the Stockholm municipal committee for animal experiments and National Institutes of Health guidelines (approved by the National Institute of Mental Health Animal Care and Use Committee).

3.1 Neuron model of a stuttering FS interneuron

Parvalbumin-positive FS interneurons have been characterized by their immunochemical, morphological and electrophysiological properties in both striatum (Kawaguchi, 1993, 1997; Taverna et al., 2007) and cortex (Kawaguchi and Kubota, 1997; Markram et al., 2004). Despite some striking differences in the organization of the cortical and striatal microcircuits, in which they are embedded, these neurons show many similarities in both areas, including a similar electrophysiological signature (see references above), a common developmental origin (Marín et al., 2000) and the coupling via gap junctions (Galarreta and Hestrin, 1999; Beierlein et al., 2000; Amitai et al., 2002; Koós and Tepper, 1999; Fukuda, 2009). Therefore, to model the stuttering in striatal FS interneurons, the channel descriptions of a previously published cortical one-compartment model was used (Golomb et al., 2007). This model contained the following voltage-dependent ionic channels, which have also been reported to be expressed in the rat striatum (Lenz et al., 1994; Weiser et al., 1994; Chung et al., 2000; Kotaleski et al., 2006): a fast sodium (Na^+) window current (I_{Na}), a fast delayed rectifier potassium (K^+) current (I_{Kdr}), and a slowly inactivating (d-type) K^+ current (I_{Kd}). The d-type current has been shown to delay spike initiation (Goldberg et al., 2008), which is also observed in many striatal FS interneurons (Plenz and Kitai, 1998a). With a small Na^+ window current and a sufficiently large d-type K^+ current, the model was able to generate the typical subthreshold oscillations (40–50 Hz) and stuttering episodes in response to somatic current injections as observed in striatal FS interneurons. The half-maximum potential for the sodium current was set to $\theta_m = -22$ mV and the d-type conductance to $g_{KD} = 1.6$ mS/cm^2 (see also Golomb et al., 2007). Some experiments were also performed with a model neuron that produces tonic discharge ($\theta_m = -28$ mV, $g_{KD} = 0.39$ mS/cm^2). To induce oscillatory fluc-

tuations in the subthreshold membrane potential and during the interburst episodes, a Gaussian white noise current with zero mean and 15 pA standard deviation (0.1 ms time step) was applied to the model neuron (Golomb et al., 2007).

In order to model distal synaptic input and dendritic gap junctions, the original one-compartment model of Golomb et al. (2007) was extended by a dendritic tree consisting of three identical sub-trees (cf. Kotaleski et al., 2006). Each sub-tree comprised one primary, two secondary, and four tertiary dendrites (i.e. each of the primary and secondary dendrites branched into two daughter arms). To allow for the same high firing rates as in the original one-compartment model, the active conductances were increased by a factor of 2 in the morphologically extended model with active primary dendrites. For the study of electrical coupling in a pair of FS neurons, the FS model cell was implemented in Parallel GENESIS (Bower and Beeman, 1998) to allow the use of parallel computing (step size, 10 μs).

3.2 Synaptic input and electrical coupling in the model

The FS neuron model included α-amino-3-hydroxyl-5-methyl-4-isoxazole-propionate (AMPA) and fast γ-aminobutyric acid (GABA) synapses. The presence of N-methyl-D-aspartate (NMDA) synapses in the model was tested with no significant changes observed (data not shown). All synapses received independent inputs in the form of random Poisson spike trains. AMPA synapses were distributed over all 127 compartments (Kotaleski et al., 2006). If NMDA synapses were present, they were located in the same compartments and received the same input as the AMPA synapses. GABA synapses were located more proximally, resulting in a total number of 31 inhibitory synapses. Measurements of spontaneous activity in organotypic cultures *in vitro* have shown that FS neurons receive a similar ratio between inhibitory and excitatory currents during an up-state (Blackwell et al., 2003). Therefore, to compensate for the smaller number of inhibitory synapses, the activation rate per GABA synapse was approximately threefold higher than for AMPA synapses. This was equivalent to using three GABA synapses per proximal compartment and activating them at the same rate as AMPA, since we used the non-saturating synapse model *synchan* in GENESIS. The time constants of the double-exponential function, which described the evolution of

the synaptic conductances in this model, were $\tau_1 = 0.7$ ms, $\tau_2 = 2$ ms for AMPA, $\tau_1 = 1.3$ ms, $\tau_2 = 4$ ms for GABA, and $\tau_1 = 3.6$ ms, $\tau_2 = 116$ ms for NMDA synapses, respectively (Hjorth et al., 2009).

Gap junctions between two FS neurons were modeled as conductive elements between the soma, the outer proximal dendrites, or the outer secondary dendrites. The conductance of a single gap junction was set to 0.5 nS, a value within the range of gap junction conductances in cortical FS neurons (Galarreta and Hestrin, 2002). A single soma-somatic gap junction resulted in a coupling coefficient of ∼11% in our model, which was within the range of coupling coefficients reported in the striatum (Galarreta and Hestrin, 2001; Koós et al., 2004). In order to obtain the same coefficient for the dendro-dendritic coupling, the number of gap junctions on the primary and secondary dendrites was increased to two and three, respectively.

3.3 Modeling of the FS-to-MS synaptic dynamics

For the FS-to-MS connections, data from rat was used recently published by Planert et al. (2010). In short, synaptic connections were identified and characterized by stimulation of a presynaptic FS cell with a train (10, 20, or 40 Hz) of 8 strong and brief current pulses (0.5–2 nA, 3 ms), followed by a so-called recovery test pulse approximately 550 ms after the end of the train, all reliably eliciting action potentials (APs). Postsynaptic neurons were held near −80 mV to ensure strongly depolarizing responses to GABAergic input. For the analysis of synaptic properties, average postsynaptic traces over multiple repetitions were examined for the existence of synaptic responses (Planert et al., 2010).

Short-term synaptic depression was modeled using a scheme described by Markram et al. (1998), where the synapse is assumed to have a limited amount of resources which is slowly restored over time (see also Tsodyks et al., 1998). The amplitude of a postsynaptic potential, PSP_n, in response to the nth AP in a spike train is a product of the fraction of available resources, R_n, and a facilitating utilization factor, u_n, scaled by the absolute synaptic efficacy, A_{se}:

$$PSP_n = A_{se} R_n u_n.$$

The utilization factor is increased by each AP and decays back towards U in the time between APs:

$$u_{n+1} = u_n \exp\left(-\frac{t_{ISI}}{\tau_F}\right) + U\left[1 - u_n \exp\left(-\frac{t_{ISI}}{\tau_F}\right)\right]$$

with $u_1 = U$. t_{ISI} denotes the time between the nth and $(n+1)$th AP. Each AP utilizes the fraction u_n from the synaptic resources, R_n, which then recovers to a value of 1 at a rate of τ_{D}:

$$R_{n+1} = R_n(1 - u_n)\exp\left(-\frac{t_{ISI}}{\tau_D}\right) + 1 - \exp\left(-\frac{t_{ISI}}{\tau_D}\right),$$

with $R_1 = 1$. The parameters U, τ_{D}, and τ_{F} were fitted to the experimental traces using a two-step process. First, the amplitudes were extracted by fitting an exponential decay to the previous response and subtracting it from the new response. The second step in the parameter fitting performed a grid search (range 0–5 s for $\tau_{\mathrm{D,F}}$ and 0–1 for U). The error was defined as the weighted sum of the absolute values of the amplitude difference at each peak between the reference trace and the modeled trace. The initial response and the recovery test response (RTR) were weighted five times stronger, and the second response was weighted double. This was done to prevent the first set of inputs from dominating over the RTR. The parameters were fitted to a train of spikes at 20 Hz and verified for some synapses at 10 and 40 Hz.

3.4 Organotypic slice cultures

Paper II describes in detail the culture preparation for organotypic cortex-ventral tegmental area (VTA) cultures on multielectrode arrays (MEAs). For the triple cortex-striatum-substantia nigra pars compacta cultures that were used in this thesis, the same protocol was followed. However, instead of the VTA, tissue from the striatum and the substantia nigra pars compacta was used. For the culture preparation on either MEA carriers or glass coverslips, coronal slices from rat cortex (350 μm thick, postnatal day 0–2; Sprague Dawley), striatum (500 μm thick), and midbrain (substantia nigra pars compacta; 500 μm thick) were cut on a vibratome (VT1000 S, Leica, Wetzlar, Germany) in sterile Gey's balanced salt solution (0.4% D-glucose)

and cultured on carriers that were coated with poly-D-lysine and treated with plasma/thrombin to allow proper tissue adhesion (Plenz et al., 2011). Carriers were either coverslips for the calcium imaging experiments, or 60-channel, planar microelectrode arrays for the recording of local field and multi-unit activity (see below). After tissue adhesion to the carrier, standard culture medium was added (600–1200 μl of 50% basal medium, 25% HBSS, 25% horse serum, 0.5% glucose, and 0.5% of 200 mM L-glutamine; Sigma-Aldrich) and changed every 3–4 days *in vitro* (DIV). At 1, 8, and 20 DIV, 10 μl mitosis inhibitor (0.3 mM uridine, 0.3 mM ARA-C cytosine-β-D-arabinofuranoside, and 0.3 mM 5-fluoro-2'-deoxyuridine) was added for 24 h to prevent excess glia cell formation. Triple-cultures were incubated at 35.5±0.5°C. Cultures on coverslips were incubated in a roller tube incubator (0.6 rotations·min^{-1}), and MEA cultures were incubated on a rocking storage tray (±75°, 0.25 cycles·min^{-1} to allow oxygenation during the first two weeks *in vitro* and for the developmental recordings; ±25°, 0.6 cycles·min^{-1} during the recording sessions for all other experiments).

3.5 Multielectrode recordings

Planar, titanium nitride microelectrode arrays with 60 channels (59 recording electrodes plus one reference electrode; 200 μm inter-electrode distance) were obtained from Multichannel Systems (Reutlingen, Germany). For the developmental recordings, a standard 8×8-layout was used. For all other MEA recordings a custom layout with two sub-arrays for cortex (4×8, 31 electrodes) and striatum (5×6, 28 electrodes) was used. Both sub-arrays were separated by 1200 μm (Fig. 6A, p. 31).

Spontaneous activity for the developmental data (20 min) and the experiments with drug bath application (60 min), was recorded in culture medium under sterile conditions. Washout recordings were done 24–48 h after the culture medium was replaced with conditioned medium collected 3–4 days before the experiment. For all other experiments, cultures were perfused with artificial cerebrospinal fluid (ACSF; bubbled with 95% O_2 and 5% CO_2; flow rate ∼100 ml/h), containing (in mM): 124 NaCl, 3.5 KCl, 10 D-(+)-glucose, 26.2 $NaHCO_3$, 0.3 NaH_2PO_4, 1.2 $CaCl_2$, and 1 $MgSO_4$. Washout conditions were recorded 10–20 min after the drug application ended. All recordings were done at 34–35°C.

3.6 Local field potential and multi-unit analysis

Data for multi-unit (MU) spike analysis was recorded at 25 kHz using the MC_RACK software (Multichannel Systems). MU spike activity was bandpass filtered between 300–4000 Hz, and spikes were detected by applying a negative threshold (–5 standard deviations, SD). Local field potential (LFP) activity was recorded at, or downsampled to 1 kHz, and subsequently bandpass filtered at 1–50 Hz if not mentioned otherwise. Negative LFP (nLFP) deflections were detected by finding the minimum value of the LFP signal that crossed a threshold of z SD. The SD was determined for each channel individually. For the analysis of the developmental data with $\pm 75^\circ$ incubation, the SD value was the standard deviation of the entire signal. For all other data sets, the SD was determined by calculating the standard deviation of 2–3 s baseline activity. The threshold value z was varied to confirm the robustness of the results. All quantitative results are reported for $z = -4.5$.

All data was analyzed in MATLAB (Mathworks, MA, USA) using the phase-neutral filter implementation *filtfilt*, and the NEUROSHARE library[1] for data import.

For the power spectral analysis of the developmental data, time windows of ± 500 ms around negative LFP threshold crossings were analyzed. The power spectrum was calculated by using the fast Fourier transform. Averages for individual cultures were calculated across all channels and subsequently normalized (integral over the entire frequency range normalized to unity) before calculating the average over all cultures.

3.7 Detection of spatiotemporal clusters

Rasters of nLFP events that crossed a predefined threshold, z, were created by binning the nLFP times with bin size Δt (Fig. 1A and B). From the nLFP rasters, neuronal avalanches were extracted by finding clusters of nLFP events that were separated by at least one bin width. The size of a neuronal avalanche was defined as the number of active electrodes during a cluster. Multiple electrode activations were counted if an electrode was activated more than once during a cluster. Therefore, the size of a neuronal avalanche is equivalent to the number of nLFPs during the avalanche.

[1] http://neuroshare.sourceforge.net

Alternatively, avalanche size can be defined as the sum of absolute nLFP amplitudes measured in μV, resulting in a continuous distribution (Beggs and Plenz, 2003).

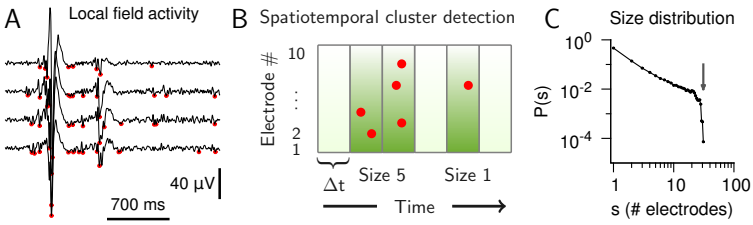

Figure 1: Detection of spatiotemporal clusters. A. Example activity from four cortical electrodes in a culture after two weeks *in vitro*. Red dots indicate significant negative deflections (-4.5 standard deviations). B. Illustration of the algorithm to detect spatiotemporal clusters. Red dots indicate nLFPs and are considered to be member of the same cluster unless separated by at least one empty bin (light green). C. Cluster size distribution from a recording with 31 electrodes (gray arrow).

To quantify the propagation of spontaneous neuronal activity, we used the branching parameter σ (Beggs and Plenz, 2003) defined as the number of nLFPs in the bin following the first bin of each avalanche divided by the number of nLFPs in the first bin. In Paper V, the bin size, Δt, was varied between 1–16 ms, and the Δt was chosen that resulted in σ equal to unity ($\Delta t = 2-4$ ms; $\sigma = 0.99 \pm 0.03$, mean $\pm$ standard deviation).

3.8 Finite-size scaling analysis

In scale-free systems, the maximum event size is not limited by the dynamics of the system but only by the system's finite size (Bak et al., 1988; Jensen, 1998). We systematically varied the number of channels for the avalanche detection and studied the probability distribution of normalized cluster sizes, $z = s/N$, where N denotes the finite number of channels in the (sub-) array. Rescaled sizes z are expressed in units of system size N and are no longer integers.

Here, we write the PMF for z as $P_z(z) = A(N)z^{\alpha}$, where $A(N)$ is the normalization factor that depends on N. With $s = 1, 2, \ldots, N$ and the property

$$\sum_{s=1}^{N} P_z(s/N) = 1,$$

one obtains

$$A(N) = \frac{N^\alpha}{1 + 2^\alpha + \cdots + N^\alpha}. \tag{1}$$

Dividing $P_z(z)$ by $A(N)$ gives z^α, which is independent of N. Thus, the transformation $P_z(z)/A(N) = P(s)/A(N)$ results in a collapse for power law distributions with slope parameter α, where $P(s) = s^\alpha/(1 + 2^\alpha + \cdots + N^\alpha)$ denotes the normalized PMF for cluster sizes $s = 1, 2, \ldots, N$. For a derivation of this result and of Eq. 1, see the Supporting Information (Text S1 in the appendix). For the empirical distributions, we fitted the slope parameter α in Eq. 1 individually for each system size N using Kolmogorov-Smirnov estimation (see below).

3.9 Statistical analyses and parameter estimation

For the cluster size distributions in neuronal avalanches, we tested the power law model — indicative of long-range spatiotemporal correlations — against the alternative of an exponential distribution, which would be expected from uncorrelated, random activity (for an identical rate between channels it would be the binomial distribution). We also compared the power law to the lognormal distribution as both are heavy-tailed, a property that can make them difficult to distinguish (Malevergne et al., 2009; Levy, 2009; Eeckhout, 2009; Mitzenmacher, 2004). In addition, we performed a comparison for the power law with exponential cutoff ("truncated" power law), the gamma and the inverse Gaussian distribution.

Power law distribution. The probability mass function (PMF) for the discrete power law (Pareto distribution) is

$$P_\alpha(s) = \begin{cases} cs^\alpha & \text{for } s_{\min} \le s \le s_{\max}, \\ 0 & \text{otherwise,} \end{cases} \tag{2}$$

with exponent, i.e., slope parameter, $\alpha < -1$. For the probability functions, we use the parameter symbols as index to denote the corresponding model, which for the power law is the symbol α. The constant $c = 1/\sum_{s=s_{\min}}^{s_{\max}} s^{\alpha}$ normalizes the PMF, such that $\sum_{s=s_{\min}}^{s_{\max}} P_{\alpha}(s) = 1$. The definition of the theoretical PMF in Eq. 2 requires a lower bound $s_{\min} > 0$, since $P_{\alpha}(s)$ diverges for $s = 0$, but can be written with an upper bound $s_{\max} = \infty$. For the cluster size distributions in this study, however, $s_{\max}$ was determined by the finite system size, i.e., the finite number of electrodes in the recording array. Thus, parameter estimates and log-likelihood ratios are reported for the range of sizes from $s_{\min} = 1$ to $s_{\max} =$ total number of electrodes in the array. In any case, the probability function in the range $s_{\min}$ to $s_{\max}$ has to be normalized to unity for both the empirical and theoretical PMF.

Exponential distribution. The PMF for the exponential distribution with parameter $\lambda > 0$ is

$$P_{\lambda}(s) = \begin{cases} ce^{-\lambda s} & \text{for } s_{\min} \leq s \leq s_{\max}, \\ 0 & \text{otherwise,} \end{cases}$$

with normalization constant $c = 1/\sum_{s=s_{\min}}^{s_{\max}} e^{-\lambda s}$.

Lognormal distribution. The PMF of the lognormal distribution is given by

$$P_{\mu,\sigma}(s) = \begin{cases} \frac{c}{\sqrt{2\pi}\sigma s} \exp\left[-\frac{1}{2}\left(\frac{\ln s - \mu}{\sigma}\right)^2\right] & \text{for } s_{\min} \leq s \leq s_{\max}, \\ 0 & \text{otherwise,} \end{cases}$$

with dispersion parameter σ, location parameter $\mu \geq 0$ and proper normalization c.

Power law distribution with exponential cutoff. The power law distribution with exponential cutoff ("truncated" power law) is given by

$$P_{\alpha,\lambda}(s) = \begin{cases} cs^{\alpha}e^{-\lambda s} & \text{for } s_{\min} \leq s \leq s_{\max}, \\ 0 & \text{otherwise,} \end{cases}$$

with $\lambda \geq 0$ and proper normalization constant c.

Kolmogorov-Smirnov (KS) estimation. The KS-statistic is based on cumulative distribution functions. For the empirical CDF of data $\mathbf{x} = (x_1, \ldots, x_n)$, $C_{\text{emp}}(s)$, and a power law distribution, $C_\alpha(s)$, the KS-statistic is defined as

$$D(\mathbf{x}; \alpha) = \max_s |C_{\text{emp}}(s) - C_\alpha(s)|. \tag{3}$$

Minimizing the objective function in Eq. 3 yields an estimate for the slope parameter α of the power law model (estimates for other model distributions can be obtained analogously):

$$\hat{\alpha} = \arg\min_\alpha D(\mathbf{x}; \alpha). \tag{4}$$

Maximum likelihood (ML) estimation. The likelihood of the power law model with parameter α, given the sample of cluster sizes, $\mathbf{x} = (x_1, \ldots, x_n)$, is

$$L(\alpha|\mathbf{x}) = \prod_{i=1}^{n} P_\alpha(x_i). \tag{5}$$

For numerical convenience, maximum likelihood and likelihood ratios are calculated with logarithmically transformed values of $L(\alpha|\mathbf{x})$. The log-likelihood is given by

$$\ell(\alpha|\mathbf{x}) = \sum_{i=1}^{n} \ln P_\alpha(x_i). \tag{6}$$

An estimate, $\hat{\alpha}$, of the power law exponent for data $\mathbf{x}$ can then be obtained by maximizing the log-likelihood function in Eq. 6 (see, Pawitan, 2001 and Hald, 1999):

$$\hat{\alpha} = \arg\max_\alpha \ell(\alpha|\mathbf{x}). \tag{7}$$

Maximum likelihood estimates for all other models can be obtained analogously (Eqs. 5 to 7).

For the minimization of Eq. 4 and the maximization of Eq. 7, we applied the Nelder-Mead method (Press et al., 2007). Here, the *fminsearch* implementation in MATLAB was used. For all models, different initial values

were tested and the algorithm was tested for convergence. For example, for the power law, initial conditions between –1 and –2 were found to give the same optimal solution. To assure the validity of the optimization results, objective functions were also studied by a grid search method for a wide range of parameter values.

Log-likelihood ratio test. The log-likelihood ratio for the power law and exponential distribution was defined as

$$LLR(\mathbf{x}) = \ell(\alpha|\mathbf{x}) - \ell(\lambda|\mathbf{x}), \tag{8}$$

where $\mathbf{x} = (x_1, \ldots, x_n)$ is the sample of cluster sizes, and the α and λ are ML estimates of the power law and exponential distribution, respectively (cf. Eq. 7). If $LLR(\mathbf{x})$ is significantly larger than zero then the power law is considered to be the better model for data $\mathbf{x}$ when compared to the exponential distribution. Conversely, if $LLR(\mathbf{x})$ is significantly smaller than zero, the exponential distribution is the better fit. The p-value for the LLR test is given by

$$p = \mathrm{erfc}\left(\frac{|LLR|}{\sqrt{2n\sigma^2}}\right), \tag{9}$$

where

$$\sigma^2 = \frac{1}{n}\sum_{i=1}^{n}\left[\left(\ell(\alpha|x_i) - \bar{\ell}_\alpha\right) - \left(\ell(\lambda|x_i) - \bar{\ell}_\lambda\right)\right]^2,$$

with $\bar{\ell}_\alpha = \ell(\alpha|\mathbf{x})/n$ and $\bar{\ell}_\lambda = \ell(\lambda|\mathbf{x})/n$ (Clauset et al., 2009). Here, we used a significance level of 0.01. The LLR for the comparison of the truncated power law with the other model distributions can be calculated analogously (Eqs. 8 and 9).

All statistical tests are denoted in the text or figure legends. Values are expressed as mean ± standard error of the mean if not stated otherwise.

3.10 Calcium imaging

Calcium imaging was performed on coverslip cultures loaded with 50 μM Oregon Green 488 BAPTA-1 (OGB; Life Technologies, NY, USA) and per-

fused with ACSF (bubbled with 95% O_2 and 5% CO_2; flow rate 100 ml/h). OGB was dissolved in 10 μl pluronic F-127 (20% in DMSO; Life Technologies, NY, USA) and 790 μl freshly prepared ACSF (Ikegaya et al., 2005; Grewe et al., 2010). Cultures were incubated for 60–90 minutes in a roller tube incubator and washed in ACSF for 10–30 minutes before imaging. Image sequences (12 bit, 2×2 binning, 320×240 pixels) were acquired with a Peltier-cooled CCD camera (Imago from TILL Photonics, Gräfelfing, Germany) on an inverted microscope (Olympus IX70) with a 20× water-immersion objective (Olympus UApo/340, numerical aperture 0.7). Excitation wavelength was set to 492 nm using a monochromator (Polychrome II, TILL Photonics). Excitation, dichroic and emission filters from Omega Optical (Brattleboro, VT, USA) were XF1087 (445–495 nm band-pass), XF2077 (reflection <500 nm), and XF3105 (508–583 nm band-pass), respectively. Image sequences of up to 320 s (7000 frames) were obtained at a rate of 21.7 frames/s (cycle time 46 ms, exposure 28 ms) using the TILLVISION 4.0 software (TILL Photonics), converted into TIF file format after acquisition and analyzed in MATLAB.

Regions of interest (ROIs) were manually selected by identifying typical cell bodies, and background subtraction was performed by automatically subtracting the fluorescence signal from a dark background region within the area of two cell body diameters. All fluorescence values are expressed as relative change in fluorescence from baseline, denoted by $\Delta F/F$ and measured as percentage. Formally, $\Delta F/F$ is defined as the change in fluorescence over baseline, that is, $\Delta F/F = (F_{\mathrm{ROI}} - F_0)/F_0$, where F_{ROI} and F_0 denote the background-corrected fluorescence intensities in the ROI and of the baseline (calculated from a 30-second sliding window), respectively. To allow for a more robust detection of calcium transients, successive increases in fluorescence ($\Delta F_{t+1} > \Delta F_t$) were summated and the threshold detection was performed on this summated signal (t and $t+1$ denote the time of two subsequent image frames). The percentage of spuriously detected $\Delta F/F$-peaks was lower than 0.5% ($n = 8$ neurons).

3.11 Pharmacology

Picrotoxin (PTX; Sigma-Aldrich, St. Louis, MO), a $GABA_A$-receptor antagonist, was dissolved in ACSF at a final concentration of 100 μM for local

drug application. Fresh solutions were prepared daily. For bath application, a 400 μM solution was prepared and dissolved in culture medium at a final concentration of 4 μM.

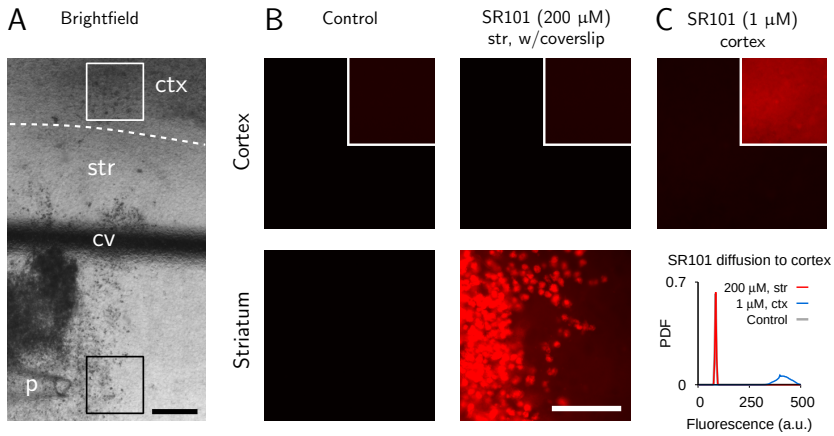

Figure 2: Two-compartment chamber for locally confined drug application as confirmed by dye staining with sulforhodamine 101 (SR101). A. Brightfield image of a cortex-striatum-substantia nigra culture showing cortex (ctx), striatum (str), coverslip (cv) for compartmentalization of the bath, and the pipette (p) for dye/drug application. The white dashed line shows the approximate border between cortex and striatum. The white and black squares show approximate locations of the imaging regions for cortex and striatum, respectively. ACSF flow was from cortex to striatum. Scale bar, 200 μm. B. SR101 staining in cortex and striatum with coverslip compartmentalization. Left panels: Minimal autofluorescence under the given imaging conditions (no pipette in bath). Inset shows the same image with increased gain for comparison with (C). Middle panels: local application of 200 μM SR101 stained glia cells in the striatal but not the cortical compartment. Scale bar, 100 μm. C. Top panel: local application of diluted SR101 (1 μM) in the cortical compartment increased fluorescence and labeled previously unstained processes (inset). Same intensity scale as in (B). Bottom panel: probability density function (PDF) of the fluorescence intensity in the cortical region. Control condition and application of 200 μM SR101 in the striatal compartment resulted in almost identical (i.e., overlapping) PDFs. Focal application of diluted SR101 in the cortex (1 μM, ctx) strongly increased fluorescence.

Local drug application in the striatum was done in a two-compartment chamber in which a glass coverslip separated the bath between the cortical and striatal tissue (see Fig. 2 above). PTX (100 μM) was applied with a glass pipette (80–100 μm tip opening) at a rate of 12 μl/min. The glass coverslip was $\sim$300 μm above the tissue and sealed with agar pieces at the side of the recording chamber. ACSF flow was directed away from the cortex to avoid drug spillover to the cortical tissue.

3.12 Immunohistochemistry and confocal imaging

A sub-set of cultures was used for post-hoc immunostaining of tyrosine hydroxylase (TH). Cultures were rinsed in phosphate buffered saline (PBS), fixed in 4% paraformaldehyde for 40–60 minutes, and incubated for 2 hours at room temperature in blocking solution (10% normal goat serum and 0.5% Triton X-100 in PBS). For all subsequent steps, a carrier solution consisting of 1% normal goat serum and 0.3% Triton X-100 in PBS, was used. Cultures were incubated for ∼12 hours at 4° in a TH-antibody solution (1:1000, anti-mouse, Immunostar, WI, USA), washed three times for 10 minutes each, incubated 1–2 hours at room temperature in secondary antibody solution (1:1000, Alexa 555 anti-mouse, Invitrogen, NY, USA), and washed again three times for 10 minutes each at room temperature. Before the confocal imaging, cultures were rinsed in PBS and mounted on coverslips using a fluorescence-preserving mounting medium (Vector Laboratories, CA, USA).

Confocal images were obtained with a Zeiss LSM 510 using a 63× oil immersion objective (numerical aperture 1.4, 0.6 μm optical thickness).

4 Results and discussion

4.1 The influence of input fluctuations on the firing patterns in FS interneurons (Paper I)

In the first part of Paper I, we investigated the influence of input fluctuations on the firing pattern in striatal fast-spiking (FS) interneurons. In awake behaving animals, these neurons show an irregular firing pattern with highly variable interspike intervals (Berke, 2008). The source of this firing variability could originate from the input that these neurons receive (Lapper et al., 1992; Wilson, 2004) and/or from intrinsic cellular properties such as the ones underlying the random stuttering discharge observed in many FS neurons in response to steady current inputs (Kawaguchi, 1993; Plenz and Kitai, 1998a; Bracci et al., 2003; Taverna et al., 2007). Using whole-cell patch-clamp recordings, we measured the voltage responses of striatal FS neurons that were subject to current injections with varying degree of fluctuations, that is, from random (Poisson-like, $q_{DC} = 0$) to constant ($q_{DC} = 1$; Fig. 3A). The behavior of a typical striatal FS cell with increasing levels of membrane depolarization and increased spike clustering for more steady input is shown in Fig. 3B (the fraction of spikes that were part of spike clusters increased from 0.05 ± 0.01 for $q_{DC} = 0$ to 0.83 ± 0.07 for $q_{DC} = 1$, $p < 0.001, n = 5$, unequal variance t-test).

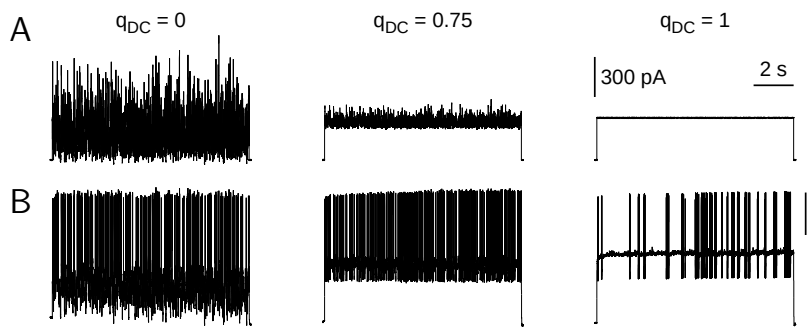

Figure 3: A. Current traces with varying degree of fluctuations, ranging from $q_{\mathrm{DC}} = 0$ (Poisson-like input, left) to $q_{\mathrm{DC}} = 1$ (steady input, right). B. Voltage traces of a striatal FS neuron *in vitro* in response to the somatically applied current traces in (A). Scale bar, 30 mV.

In addition, the spike discharge that was random across trials for stuttering FS neurons in response to steady input became very reliable when the neurons received fluctuating input (Fig. 4). This behavior was reported previously in pyramidal cells (Mainen and Sejnowski, 1995) and might constitute a more general property of various neuron types (Schneidman et al., 1998; La Camera et al., 2006).

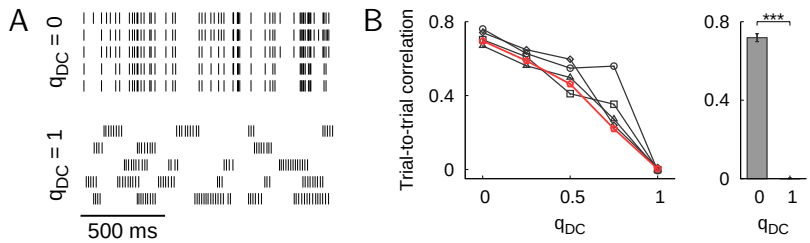

Figure 4: A. Example rastergram for a striatal FS neuron *in vitro* that received five identical trials of fluctuating input ($q_{DC} = 0$, top rasters) and steady input ($q_{DC} = 1$, bottom rasters). B. Summary for $n = 5$ striatal FS neurons (left panel, black lines) and the model cell (red line, see text below). The difference between $q_{DC} = 0$ and $q_{DC} = 1$ was statistically significant ($^{***}p < 0.001$, $n = 5$ striatal neurons, unequal variance t-test). Error bars denote standard deviations.

FS neurons have been shown to be coupled by electrical synapses (Kita et al., 1990; Tepper et al., 2004; Fukuda, 2009), which can influence spike synchronization among coupled neurons as suggested by modeling studies (Nomura et al., 2003) and experimental evidence *in vitro* (Galarreta and Hestrin, 1999; Gibson et al., 2005; Mancilla et al., 2007). However, simultaneous recordings from striatal FS neurons *in vivo* (Berke, 2008), and a recent modeling study that used a model of a tonically firing FS cell (Hjorth et al., 2009), suggest that spike synchronization is not a prevailing feature of FS firing in the striatum. In the second part of Paper I, we tested if this prediction would hold for a model of electrically connected FS stuttering neurons (Golomb et al., 2007). The FS model was in agreement with our *in vitro* measurements (i.e., level of depolarization, percentage of clustered spikes, and trial-to-trial correlation; cf. Fig. 4B, black lines: striatal neurons, red line: model). In line with observations *in vivo* (Berke, 2008) and in a model of tonically firing FS neurons, we found little spike synchronization in the stuttering FS model when the neurons were driven by fluctuating in-

put ($q_{DC} = 0$). Together with the lack of spike synchronization *in vivo*, this result suggests that the firing variability in striatal FS neurons *in vivo* most likely originates from fluctuations in the input to these neurons.

In the last part of Paper I, we investigated the influence of firing variability in FS neurons *in vivo* on the variability of postsynaptic responses in a model of FS-to-medium spiny (MS) synapses. The dynamics of FS-to-MS synapses is characterized by strong depression (Plenz and Kitai, 1998a; Koós et al., 2004; Gustafson et al., 2006; Gittis et al., 2010; Planert et al., 2010), that is, repeated synaptic release results in diminished synaptic efficacies. Fig. 5A shows simulated postsynaptic potentials (PSPs) of a FS-to-MS synapse in response to an *in vivo* FS spike train. The presence of spike clusters and spike pauses led to a wide range of PSP amplitudes.

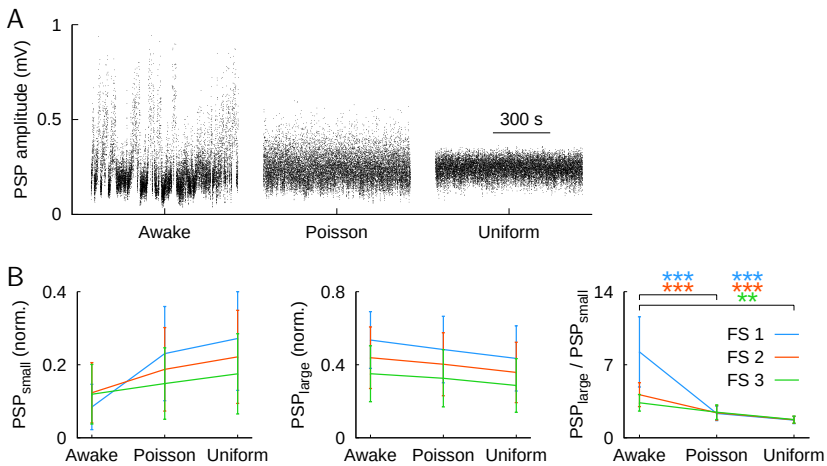

Figure 5: Influence of natural FS firing discharge on the PSP distribution in MS neurons. A. Distribution of simulated PSPs for a typical FS-to-MS synapse in response to an *in vivo* FS spike train. For the original spike train (awake), the distribution of PSPs covered the widest range, i.e., from very small (depressed synapse) to almost maximum (fully recovered; maximum possible PSP for this synapse was ∼1 mV). B. Summary of depressed PSPs (PSP_{small}), recovered PSPs (PSP_{large}), and the ratio PSP_{large}/PSP_{small} for 11 synapses and three FS neurons ($^{**}p < 0.001$, $^{***}p < 0.0001$, Kruskal-Wallis test with Tukey-Kramer multiple comparison). Error bars denote standard deviations.

In contrast, shuffled spike trains did not have the extended pauses and spike clusters that were present in the original data, and consequently resulted in a smaller range of PSP amplitudes (Fig. 5).

The synaptic dynamics of the model was derived from paired *in vitro* recordings (Planert et al., 2010). Although synaptic depression might be less pronounced *in vivo* (Reig et al., 2006; Reig and Sanchez-Vives, 2007), the qualitative behavior in Fig. 5 is not expected to change. This assumes that mainly the synapse utilization factor changes and that the recovery time constant for the synaptic depression remains larger than the short interspike intervals within spike clusters.

Together, the results from Paper I suggest that input fluctuations in striatal FS neurons significantly contribute to the firing variability observed *in vivo*, and ultimately to the variability of postsynaptic efficacies in striatal MS output neurons. Striatal FS neurons receive input from multiple sources, including cortex, thalamus and basal ganglia (Wilson, 2004). In the following sections, the dynamics of the cortex and striatum are studied in more detail in organotypic cortex-striatum-substantia nigra pars compacta cultures.

4.2 Organotypic cortex-striatum-substantia nigra pars compacta cultures (Paper II)

Paper II describes a protocol for the preparation of organotypic cultures on planar multielectrode arrays (MEAs) for the recording of cortical neuronal avalanches (Beggs and Plenz, 2003; Shew et al., 2009; Yang et al., 2012). Many steps of the culture preparation on MEAs are identical to the protocol for culture growth on coverslip glass (Plenz and Kitai, 1998a), such as the coating of the carriers with poly-D-lysine to enhance tissue binding to the surface, the preparation of solutions and culture medium, the dissection of the tissue pieces, and the strict adherence to sterile preparation and culture conditions in the absence of any antibiotics, which are known to affect neuronal activity. However, other aspects of the protocol are precisely adjusted to the properties of the MEAs. One critical parameter is the exposure of the tissue to both medium and oxygen. For organotypic cultures on semiporous membranes, this condition is given at the interface between medium and air (Stoppini et al., 1991; Gähwiler et al., 2001). Cultures in roller tubes are exposed to medium and air in an alternating fashion (Plenz and Kitai, 1998a; Gähwiler et al., 2001). For organotypic cultures on MEAs, an incubator with precisely controllable tilt and rocking trajectory was used to op-

timize growth and developmental conditions, that is, to achieve appropriate alternating exposure to culture medium and air with minimal mechanical disturbances. Under proper culture conditions, healthy tissue shows thinning from initially 500 μm in case of the striatum, to ∼50 μm after 2–3 weeks without the appearance of necrosis. Fig. 6A shows an organotypic triple-culture on a 59-electrode array after two weeks *in vitro*.

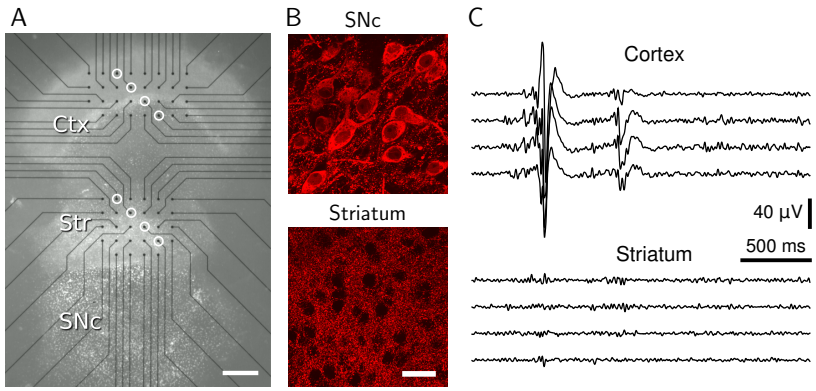

Figure 6: A. Organotypic cortex-striatum-substantia nigra pars compacta culture after 14 days *in vitro* (Ctx, cortex; Str, striatum; SNc, substantia nigra pars compacta). The white circles indicate the electrodes for which representative local field potentials (LFPs) are shown in (C). B. Tyrosine hydroxylase immunostaining of dopaminergic neurons in the SNc (top panel, 0.8 μm optical slice) and the striatal innervation by dopaminergic fibers (bottom panel, 5 μm maximum intensity z-projection) at 14 DIV. C. Example LFP activity for four cortical and striatal electrodes (white circles in A).

Successful cultures show neuron types, neuron morphologies, and neuron electrophysiologies that are observed in other slice culture preparations and which have been shown to be very similar to that in the acute slice with spontaneous activities similar to that in *in vivo* resting conditions (Plenz and Aertsen, 1996a; Plenz and Kitai, 1998a; Klostermann and Wahle, 1999; Gähwiler et al., 2001). Some differences are, however, worth to discuss. MS neurons in organotypic cultures have a higher input resistance than in acute slices (Plenz and Kitai, 1998a; Taverna et al., 2004; Gittis et al., 2010), which could be a result of the lower spine density in culture (Gustafson et al., 2006). In addition, the lateral connections between MS neurons have a slightly increased conductance and are more numerous compared

to acute slice (Czubayko and Plenz, 2002; Gustafson et al., 2006; Tunstall et al., 2002; Taverna et al., 2004). Because the spontaneous rate of MS firing in organotypic cultures is comparable to *in vivo* data, the above differences might constitute unknown homeostatic mechanisms.

The triple culture preparation used in this thesis consists of the cortex, striatum, and substantia nigra. The latter tissue contains two parts: (i) the pars compacta part with dopaminergic neurons (Fig. 6B, top panel) that resulted in a dense fiber innervation of the striatum (lower panel) already at 14 days *in vitro* (DIV) (Plenz and Kitai, 1998b); (ii) the pars reticulata part that most likely provides a target for striatonigral MS neurons. Other brain structures important for *in vivo* brain function and considered in many basal ganglia models were not present in this preparation. If required for an experimental question, it is possible to co-culture other brain regions in organotypic cultures, such as the thalamus, globus pallidus and subthalamic nucleus (Klostermann and Wahle, 1999; Plenz and Kital, 1999). However, including additional nuclei in the organotypic culture, increases the complexity and makes certain parameters more difficult to control. Using a reduced preparation, on the other hand, requires that experimental findings are confirmed under more physiological conditions and ultimately *in vivo*.

Despite the lack of external input, organotypic cortex cultures generate spontaneous activity after 4–6 DIV that can be monitored for many weeks. Fig. 6C shows a short period of local field potentials (LFPs) from each of four cortical and striatal electrodes (white circles in Fig. 6A). In the cortex, spontaneous LFP activity organizes as neuronal avalanches, that is, scale-free activity clusters that are characterized by a power law distribution, $P(s) \propto s^{\alpha}$, of cluster sizes, s, with exponent α close to -1.5. The following section (Papers III and IV) provides the necessary framework to analyze cluster size distributions and statistically test the power law hypothesis for neuronal avalanches.

4.3 Statistical analyses of power law distributions in cortical neuronal avalanches (Papers III and IV)

Cortical neuronal avalanches are identified by a power law in avalanche size distributions. However, deciding whether an empirical probability dis-

tribution actually follows a power law can be difficult (Jones and Handcock, 2003; Goldstein et al., 2004; Clauset et al., 2009). Commonly, visual inspection and least-square fitting on logarithmically transformed data is used to determine if a given distributions is consistent with the power law hypothesis and to estimate the power law exponent (Albert et al., 1999; Liljeros et al., 2001; Beggs and Plenz, 2003). Problems with this approach arise with small sample sizes, which affects particularly the tail of the distribution, or if only a limited range of the distribution is analyzed (Goldstein et al., 2004; Newman, 2005; Malevergne et al., 2009). Furthermore, testing the power law scaling in empirical data without comparison to alternative distributions can be misleading (Clauset et al., 2009).

In Paper III, we tested the power law hypothesis for neuronal avalanches using and expanding recently suggested more stringent statistical methods (Goldstein et al., 2004; Newman, 2005; Clauset et al., 2009) that were applied to previously published data sets from organotypic cultures (Beggs and Plenz, 2003), rat *in vivo* under anesthesia (Gireesh and Plenz, 2008), and awake macaque monkeys *in vivo* (Petermann et al., 2009; Yu et al., 2011) from various cortical areas, including somatosensory, primary motor and premotor cortex. In particular, to test the power law hypothesis, we performed the following steps: (i) finite-size scaling analysis to motivate the power law model as an appropriate description for the distribution of avalanche sizes, (ii) parameter estimation of the statistical models to determine the exponent of the power law and to allow the subsequent model comparison, and (iii) comparison of the power law and the exponentially truncated power law to the alternatives of an exponential, lognormal and other distributions.

For all data sets, finite-size scaling showed a collapse of rescaled cluster size distributions as expected for power law distributed values (Fig. 7). Importantly, rescaling of time-shuffled data did not result in a collapse of the rescaled distributions (not shown). These results, which demonstrated the scale-free behavior of neuronal avalanche size distributions, motivated the next steps of the analysis, that is, parameter estimation and model comparison. Many studies used least-square fitting on log-log transformed data (Beggs and Plenz, 2003; Albert et al., 1999; Liljeros et al., 2001) to estimate the power law exponent, an approach that can suffer from the sample noise

in the tail of the distribution as pointed out previously (Newman, 2005; Clauset et al., 2009).

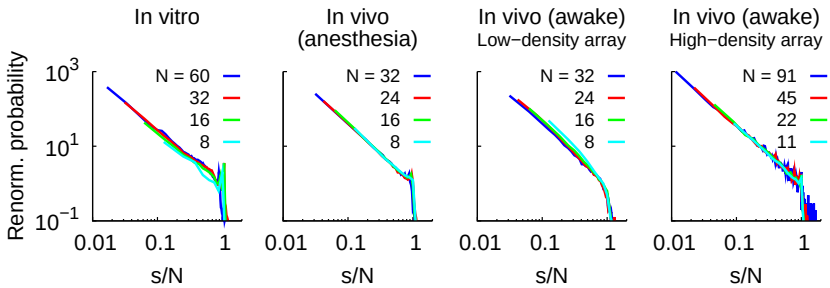

Figure 7: Collapse of rescaled cluster size distributions for average *in vitro* distributions ($n = 7$), average *in vivo* distributions under anesthesia (rat, $n = 7$), and the two awake monkeys with low- and high-density array, respectively (from left to right). All distributions showed a cutoff at the system size ($s/N = 1$).

Therefore, in Paper III, we calculated parameter estimates by using two additional methods, that is, a fit of the cumulative distribution (based on the Kolmogorov-Smirnov statistic) and likelihood maximization (Clauset et al., 2009). In line with previous reports (Beggs and Plenz, 2003; Gireesh and Plenz, 2008; Petermann et al., 2009), the power law exponent α was found to be close to -1.5 with all three methods. Importantly, to obtain accurate estimates, the cutoff at the system size (i.e., the number of electrodes in the multielectrode array, Fig. 7) had to be taken into account. The existence of the cutoff in the cluster size distributions was not only evident from the strong decrease in the probability beyond the system size (Fig. 7) but also from the comparison of avalanche size, s, and the number of unique electrodes that contributed to the avalanche (Fig. 8). Up to the system size, the size of an avalanche reflected the spatial extent (Fig. 8A, black arrow), that is, multiple participations of a single electrode were rare and s was approximately equal to the number of unique electrodes. In the model, the cutoff was incorporated by setting the upper bound, $s_{\max}$, to the system size, N, and not to infinity. In Paper IV, we compared the results obtained for the two different choices of the upper bound, since $s_{\max} = \infty$ is assumed without critical evaluation by many authors (Clauset et al., 2009; Dehghani et al., 2012).

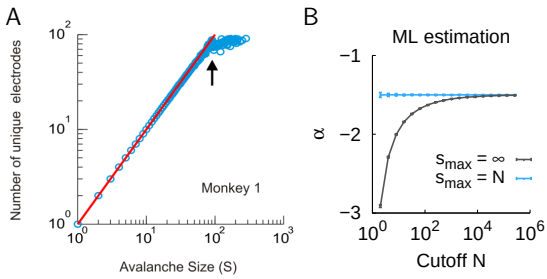

Figure 8: Ignoring the cutoff biases the estimation of the power law exponent. A. Avalanche sizes below the system size ($N = 91$, black arrow) reflect the number of unique electrodes that are part of an avalanche. Multiple electrode activations were rare and mainly observed for $s > N$. B. For synthetic power law distributions with exponent -1.5, the estimated exponent, α, is plotted as a function of the cutoff, N, which ranged from 2 to $>10^5$. Blue: estimation that takes the cutoff into account. Gray: estimation that assumes no cutoff (i.e., $s_{\max} = \infty$). For each cutoff value, 100 simulations were performed. The data are represented as mean±standard deviation.

In Fig. 8B, we used synthetic data with an underlying power law exponent of -1.5. Using the correct upper bound, $s_{\max} = N$, gave estimates of α close to -1.5 (i.e., the "true" underlying exponent) independent of N. In contrast, using $s_{\max} = \infty$ resulted in biased, more negative estimates of α for small N (Fig. 8B). Importantly, neglecting the cutoff is equally problematic when examining the complementary cumulative distribution of the data in double-logarithmic coordinates (Clauset et al., 2009; Dehghani et al., 2012). While the complementary cumulative distribution with $s_{\max} = \infty$ follows a straight line in double-logarithmic coordinates, the same underlying distribution with finite cutoff, N, does not. Instead, the complementary cumulative distribution is curved in a double-logarithmic plot and cannot be compared to a straight line. Consequently, for the proper parameter estimation and interpretation of data with finite cutoff, this cutoff needs to be incorporated in the model distribution.

To confirm that the power law was indeed a good fit to the data, we compared the power law fit to alternative distributions, such as the exponential distribution, which would be expected from random, independent activity. This was done by using a log-likelihood ratio (LLR) test (Pawitan, 2001; Clauset et al., 2009) and by a model comparison based on the Kolmogorov-Smirnov (KS) statistic. The exponential distribution did not provide valid

fits to the data as evident from visual inspection (Fig. 9A) and additional statistical analyses.

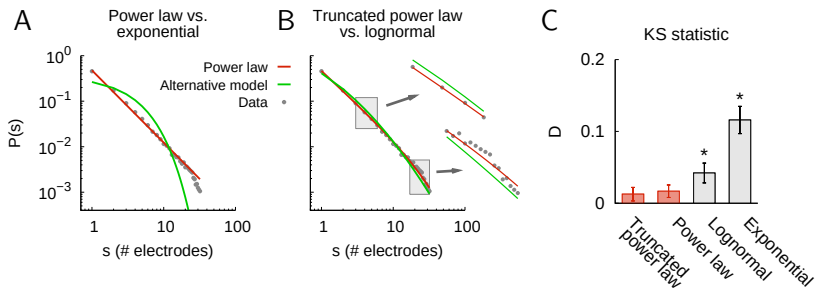

Figure 9: Model comparison using the LLR test. A. Model fits obtained by ML estimation for the power law (red) and the exponential model (green) for an *in vivo* cluster size distribution obtained in monkey cortex. B. The same for the comparison between the exponentially truncated power law (red) and the lognormal distribution as the alternative model (green). The insets show detailed views of the distributions, corresponding to the respective gray rectangles. C. Average KS distance of the model distributions for all data sets ($n = 16$, which includes 7 data sets recorded *in vitro*, 7 *in vivo* under anesthesia, and 2 *in vivo* awake). Error bars denote the standard deviation. The single-parameter power law and the power law with exponential cutoff yielded significantly better fits to the data than the lognormal or the exponential distribution ($^*p < 0.0001$, Kruskal-Wallis test and Tukey-Kramer multiple comparison).

First, the distance between the data and model distribution as measured by the KS statistic, D, was significantly smaller for the power law (Fig. 9C, power law *versus* exponential), indicating that the power law distribution provided the better fit. Second, the LLR analysis, which provides a significance value for individual data sets, showed that all LLR values ($n = 16$ data sets) were significantly in favor of the power law (LLR $= 377 - 8269$, all $p < 0.0001$). In addition, we compared the power law to other heavy-tail distributions such as the lognormal distribution. Because many finite-size systems show an exponential cutoff below the system size (Jensen, 1998), we used the power law without and with exponentially truncated tail for the model comparison (Fig. 9B,C; Supplemental Table S1 in the appendix, Paper III). The LLR test revealed that the exponentially truncated power law provided better fits than the lognormal distribution for all tested avalanche size distributions ($p < 0.01$ for 12 out of 16 data sets). In line with this result, the average KS distance between the empirical and model distributions

was smallest for the power law (with and without exponential truncation) compared to the other evaluated model distributions (Fig. 9C).

The main parameters for the analyses in Papers III and IV are the threshold for the nLFP detection and the bin size for the detection of spatiotemporal clusters. To confirm the robustness of the first parameter, we performed an LLR test for the cluster size distributions for one monkey data set and varied the threshold values from -1.5 to -5 standard deviations (Petermann et al., 2009). For all comparisons, the LLR was in favor of the power law without and with exponential cutoff when compared to the exponential and lognormal distribution, respectively. However, because more negative threshold values resulted in a smaller number of samples (i.e., avalanches), not all LLR values did reach statistical significance. For the second parameter, that is, the bin size, Δt, we applied the values that were used in the original studies (Beggs and Plenz, 2003; Gireesh and Plenz, 2008; Petermann et al., 2009; Yu et al., 2011). Because changes in Δt lead to a systematic change of the power law exponent but do not affect the scaling (Beggs and Plenz, 2003; Plenz, 2012), the above analyses are robust with respect to changes in Δt.

In summary, the results presented in Papers III and IV support the power law scaling in neuronal avalanches in many cortical areas *in vivo* and in organotypic cultures *in vitro*. The exponent $\alpha = -1.5$ together with the balanced propagation of activity (i.e., branching parameter close to unity; Plenz, 2012), provide strong evidence for critical state dynamics in cortical networks.

4.4 Intrastriatal inhibition decorrelates cortical neuronal avalanches (Paper V)

In Paper V, we studied the network dynamics in cortex and striatum in organotypic cortex-striatum-substantia nigra pars compacta cultures using cortical and striatal multielectrode recordings and calcium imaging of striatal neurons. Local field (LFP) activity was measured simultaneously from up to 31 electrodes in the cortex and 28 electrodes in the striatum. The analysis of spatiotemporal clusters revealed neuronal avalanches in the cortex as evident from power law distributed avalanche sizes with an exponent α close

to -1.5 (Fig. 10A, left panel; $\alpha = -1.47 \pm 0.02$, $n = 8$ cultures) and positive LLR values that were in favor of the power law compared to the exponential distribution (LLR $= 1564 - 27,090$, all $p < 0.001$). Accordingly, avalanche sizes when measured as the sum of absolute nLFP amplitudes, followed a continuous power law distribution (Fig. 10A, right panel).

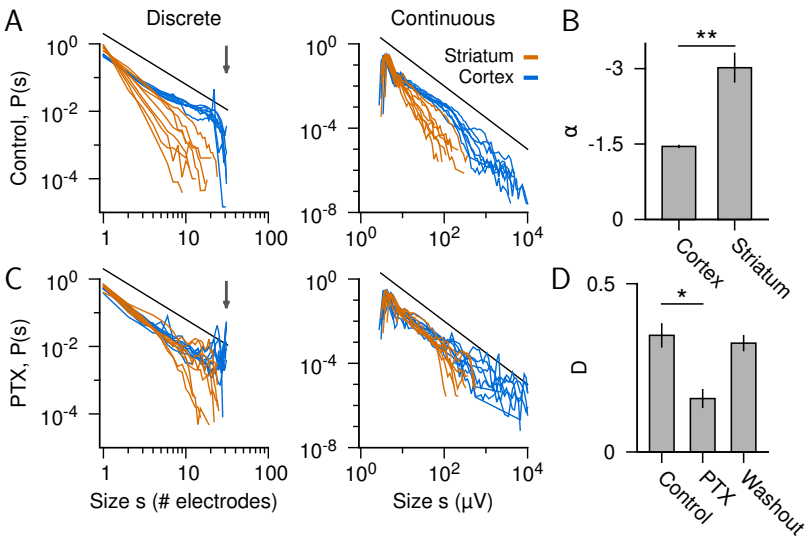

Figure 10: A. Discrete (left panel) and continuous (right panel) cluster size distributions for cortex and striatum ($n = 8$ cultures). Arrow: maximum system size for the cortical sub-array (31 electrodes). Black lines indicate a power law with $\alpha = -1.5$ for comparison. B. Average power law exponent for cortex and striatum under normal conditions ($^{**}p < 0.01, n = 8$, Wilcoxon signed- rank test). Error bars in (B) and (D) denote the standard error of the means. C. Same as in (A) with bath application of picrotoxin (PTX, 4 μM). D. Kolmogorov-Smirnov distance, D, between cortical and striatal cluster size distributions under control, PTX, and 24-hour washout condition ($^{*}p < 0.05, n = 8$, Friedman test with Bonferroni correction).

In contrast to cortical cluster sizes, the striatum showed reduced spatiotemporal correlations and power law distributions with a significantly more negative exponent at the same spatial and temporal scale ($\alpha = -3.04 \pm 0.27, p < 0.01$; see Fig. 10A,B). Although the striatum showed a smaller number of large clusters, the size distributions were consistent with a power law distribution (LLR $= 123 - 3225$ compared to an exponential distribution, all $p < 0.01$ for $n = 8$ cultures). Importantly, the difference between cortical and striatal cluster size distributions was significantly smaller in the

presence of the $GABA_A$-receptor antagonist picrotoxin (PTX; Fig. 10C,D). This demonstrates two aspects of striatal dynamics. First, dynamical differences between cortex and striatum observed under normal conditions disappear under abnormal conditions, for example, when inhibition is reduced in cortex and striatum. Second, the small probability of large striatal clusters under normal conditions does not result from an anatomical constraint of the striatum (i.e., absence of long-range connections or more flattening of the striatal tissue compared to cortical tissue in the culture system). Instead, the difference reflects dynamical differences. Thus, under normal conditions, cortical and striatal networks follow qualitatively different dynamics.

The bath application of PTX in the above experiment does not allow to distinguish between the cortical and striatal contribution to the increased probability for larger striatal activity clusters. That is, increased cortical synchronization (Yang et al., 2012) could result in a more effective drive of the striatal circuit and thus lead to larger striatal clusters. Similarly, reduced intrastriatal inhibition is likely to increase the probability of larger activity clusters in the striatum. To study the influence of intrastriatal inhibition on the activity of the MS output neurons, we measured calcium activity in striatal neurons loaded with the calcium dye Oregon Green 488 BAPTA-1 (OGB) under normal conditions and in the presence of local striatal application of PTX. Fig. 11A shows 5 min of calcium activity (measured as percentage change in fluorescence over baseline, $\Delta F/F$) in 11 striatal neurons under control and PTX condition, and ∼10 min after washout. The average amplitude of $\Delta F/F$-peaks, which was linearly related to the number of action potentials ($R^2 = 0.99, n = 8$), increased significantly under PTX (Fig. 11B). This increase was also measured after acute lesions of the SNc (Fig. 11B), indicating that it did not depend on GABAergic input from the substantia nigra (Tritsch et al., 2012). Importantly, the use of a two-compartment chamber with directed flow of ACSF prevented any significant drug spillover to the cortical tissue (see Fig. 2, p. 25). This was shown by the fact that local application of PTX in the striatum did not affect the total rate of events as measured by the number of calcium transients in the wide-field fluorescence signal (Fig. 10D). This rate of events in the striatum reflects the rate of cortical up-states that led to striatal excitation (Plenz and Aertsen, 1996b).

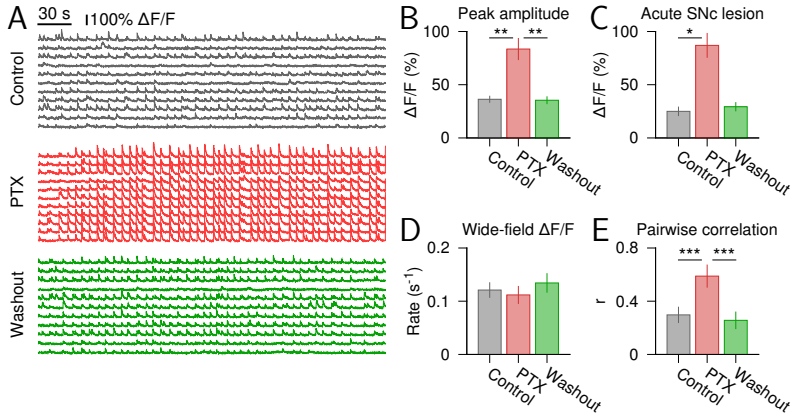

Figure 11: A. Example $\Delta F/F$ traces of 11 striatal neurons before (control), during (PTX, 100 μM), and 10 min after (washout) local drug application. B. Average $\Delta F/F$-peak amplitudes under PTX ($^{**}p < 0.01, n = 8$ cultures). C. Average $\Delta F/F$-peak amplitudes in striatal neurons after acute lesion of the substantia nigra ($^{*}p < 0.05, n = 4$). D. Global event rate as measured by the rate of $\Delta F/F$-peaks in the wide-field, striatal fluorescence signal ($p = 0.72, n = 3$). E. Average pairwise correlation for all three conditions ($^{***}p < 0.001, n = 8$). For all tests the Friedman test with post-hoc Bonferroni correction was used.

Local blockade of striatal inhibition significantly increased the correlation of calcium transients across striatal neurons (Fig. 11E) as well as the overall number of action potentials per cortical input. This result suggests that neurons in the striatal microcircuit receive correlated input from the cortex, which is decorrelated through striatal inhibition. It should be noted that the decay kinetics of OGB (at the order of hundreds of milliseconds; Kovalchuk et al., 2000; Grewe et al., 2010) does not allow to measure spike timing at a high temporal resolution. The fine temporal scale at which the striatum might receive the correlated input can therefore not be inferred from the calcium imaging (but see Stern et al., 1998).

From the known statistics of striatal neuron numbers (Oorschot, 1996; Plenz and Aertsen, 1996a), most of the imaged neurons are expected to be MS neurons as identified by morphological and electrophysiological properties (Czubayko and Plenz, 2002; Kerr and Plenz, 2004; Gustafson et al., 2006). The results in Fig. 11 can thus be considered to reflect changes in the striatal output.

That local application of $GABA_A$-receptor antagonists into the striatum *in vivo* is able to cause behavioral changes, such as motor tics and dyskinesia, has been demonstrated in various studies (Standefer and Dill, 1977; Muramatsu et al., 1990; McCairn et al., 2009). The results from Paper V suggest that in addition to the elevated activity level (which is also observed *in vivo*), increased output correlations among MS neurons could contribute to the behavioral effects. A recent study suggests that dyskinesia can be caused by a selective blockade of AMPA-mediated input to striatal FS interneurons to reduce their activity (Gittis et al., 2010). However, the reduction of FS discharge was accompanied by a dichotomous change of the firing rate in simultaneously recorded MS neurons. The increase of activity in some of the MS neurons does not allow to clearly differentiate between the contribution of the feedforward *versus* feedback inhibitory circuit. Additional experiments are necessary to elucidate the role of these two cortex-driven circuits, and the organotypic culture preparation provides a reduced and versatile system to study this question.

5 Conclusions and future perspectives

The results from this thesis show that the striatum receives spatiotemporally diverse inputs from the cortex during neuronal avalanches *in vitro*. Under normal conditions, cortical and striatal networks follow qualitatively different dynamics; whereas spontaneous local field potentials in the cortex are characterized by scale-free dynamics with long-range spatiotemporal correlations, striatal local field activity shows a significantly smaller percentage of extended activity clusters at the same spatial and temporal scale. Future studies should determine if the striatal dynamics observed during spontaneous activity in the organotypic cultures are also present during evoked activity and whether the striatum exhibits these dynamics also *in vivo*.

In the first part of this thesis (Paper I), we have shown that spike timing in striatal FS neurons is largely determined by input fluctuations, and that the resulting firing variability leads to a wide range of postsynaptic responses in MS neurons. It has been shown that MS neurons receive substantial inhibitory input during up-states (Blackwell et al., 2003; Wilson, 2007) and it would be of interest to determine the precise contribution of FS inhibition to this input by modulating their activity. Several techniques, such as electrophysiological recordings (Kerr and Plenz, 2004; Gustafson et al., 2006), pharmacological manipulations (Magazanik et al., 1997; Gittis et al., 2010) and/or optogenetics (Mattis et al., 2012; Szydlowski et al., 2013), could be used to increase or reduce FS activity.

The importance of intrastriatal inhibition in shaping striatal output is also evident from the results of the calcium imaging experiments in Paper V. These experiments indicate that intrastriatal inhibition shapes striatal activity by (i) decreasing the average number of action potentials during up-states, and (ii) decorrelating the output rate across neurons. Two questions should be addressed in future studies. First, does an increase in the striatal output correlation change the activity in downstream structures? If this is the case, it would be important to determine the striatal network dynamics under pathological conditions. For example, chronic dopamine depletion in Parkinson's disease, which causes multiple changes at the striatal level (Tseng et al., 2001; Day et al., 2006; Kreitzer and Malenka, 2007; Taverna et al., 2008; Gittis et al., 2011), also leads to increased levels of synchro-

nized activity in the external and internal segments of the globus pallidus (Nini et al., 1995; Hammond et al., 2007). It would be interesting to determine a possible role of the striatum in these pathological dynamics. Second, if disrupted striatal output does indeed affect the activity in downstream nuclei, it would be important to reveal the origin of the inhibition that appears to be crucial for normal striatal dynamics. Different striatal cell types are implicated in basal ganglia dysfunctions (Vonsattel and DiFiglia, 1998; Kalanithi et al., 2005; Gittis et al., 2010) and understanding the functional roles of these cell types in shaping striatal output under normal and abnormal conditions will bring us closer to understanding and restoring healthy brain function.

Acknowledgments

During the past few years, I encountered many amazing and truly inspiring people, and I now find it difficult to imagine what this experience would have been like had I not met them.

Thank you so much Jeanette for your great support and the freedom you gave me to explore. You were always there to help, even in situations when you just arrived back from a 12-hour flight. Thanks Gilli for your spirit and support! I hope we will find out one day where that train will go. Thank you Dietmar for teaching me how to separate signal and noise, for your support and giving me the possibility to work in such a diverse field without getting buried by an avalanche.

I am grateful to all people that contributed to the papers presented in this thesis: Dietmar Plenz, Jeanette Hellgren, Gilad Silberberg, Henrike Planert, Johannes Hjorth, Josh Berke, Craig Stewart, Woody Shew, Hongdian Yang, Tim Bellay, Shan Yu, Andrew Mitz, Richard Saunders, Oren Shriki, Aaron Clauset, Avrama Blackwell, Dieter Jaeger, and the anonymous reviewers.

I would like to thank the examiners of my halftime seminar, Joanna Tyrcha, Gilberto Fisone, Konstantinos Meletis, and Marie Carlén.

I so much enjoyed my time at the Department in Stockholm. Thank you Peter, Tatiana, Gilberto, Lennart and many others for the great Neuroscience course. I thank Sten, Abdel, Ole, Peter, Brita, Russ, Dagmar, Pasha, Isaac, André, Mia, Patrik, Ola, and Christian and many others for interesting conversations and the atmosphere that distinguishes the Department. Iris, I enjoyed to listen to your melodic whistling, and of course I thank you for all your administrative help.

I thank the many people at the Department of Computational Biology at KTH. My special thanks go to Anders Lansner, Erik Aurell, Erik Fransén, Alexander, Johannes, Jovana, Jenny, Marcus, Pradeep, Mikael D, Mikael L, and Örjan.

Many thanks also to Joanna Tyrcha and John Hertz for interesting discussions.

Jeppe, Henrike and Marcus, I will always remember my first weekend in Stockholm — at the roof in Gamla Stan. Henrike, it was a nice coincidence that we left on the same plane; thanks for your friendship and support. Marcus, let's get the boat. Thanks for your friendship and many good memories: Chus, Chus, Hui Min, Anastasia, Kim, Carolina, Ann-Charlotte, Evanthia, Jessica, Susanne, Stylianos, Gayane, Slobodan, Kai, Johannes, Valeria, Lotta, Martin, Adolfo, Ernesto, Kristoffer, Rikard, Sophia, Jens, Karin, Seth, Dave, Amilcar, Erik, Richardson, Alexandros, Jesper R, Di, Nasren, Swati, Nerijus, Loretxu, Orestis, Carmelo and Ramón. Ebba, our plants will continue to grow!

Thanks Craig for the endless hours that we spend together in our little, sterile cockpit. Shan, thank you so much for your mentoring; your work truly inspires me. Tim, I remember all the interesting things you showed me on the first day in the lab. I am thankful that we were able to share the Ying-Yang of research. Hongdian, I really enjoyed each of our conversations. Thanks Woody and Gireesh for your feedback and help. Oren, you are a great scientist and an excellent teacher; you taught me a lot. I thank you Yann for getting me started. Thanks Jeff for making me aware of the snake. Sini, your humor makes a day brighter.

Thank you Avrama, Rodrigo, Sriraman, Rebekah and Sarah for interesting discussions, and for making my visit at your lab a great experience.

I thank Paolo, Sam, Sarah, Carlo, Jonathan, Avi, Claire, Kristin, Suel-Kee, Andreas, Amritha, Nicola, Alex and all the sunny (ex-) passengers from the A,B,C pod.

Thank you Laura, Saurav, Anke, Carly, Kelly, Cecilia, Carolyn, Ray, Wangko, Jaime, Jacomijn and all the others for the many good hours during our transatlantic journey.

I am very grateful to Idan Segev and Shaul Druckman for making it possible to visit Hebrew University. Thanks Shaul for an incredibly interesting week and for showing me the optimal way to improve a model.

I thank Rusty Lansford, Cary Lai, Lief and all the others for the best summer school ever. Thanks Lotta for explaining me the basics of molecular neuroscience.

I am very thankful to Mark Stopfer, Leo Belluscio, Chris McBain, and Judie Walters for what they teach. You are a guide for me and for others.

I thank Chip Gerfen, Chris McBain and Xiaoqing Yuan for their support, the transgenic animals and antibodies. I would like to thank Carolyn Smith for teaching me the basics and details of confocal microscopy.

I want to thank Brian Wilgenburg, James O'Malley, Vanessa and Craig for their excellent veterinary advice, and the NIH animal facility for taking care of our animals.

I thank Sue O'Harra, Margarita Valencia, Richard Doucette, Karin Lagerman, Thomas Johansson, Ida Engqvist for their administrative support. Thank you Bob Innis, Bob Harris, Lennart Brodin, Vic Pike and many others for making the NIH-KI program possible.

I thank the Karolinska Institute Library and the NIH Library for their professional support.

Thanks to the free culture and open software community.

My dear DC friends: Leo, Inês, Teasel, Nick, Julio, Daniel P, Brione, Suel-Kee, Cláudia, Anke, Jesper, Laura, Daniel B, Fanny, Jake, Meg and Cameron, I am happy about all the hours that we spent together. Thanks Geoff and Bruno for sharing the enjoyment of climbing.

Thanks Jamie and Melissa, you made me curious about America, America. From you, I learned about home-made pasta, the third dimension, cuttlefish and much more.

Thank you Steven, Anne, Ami and Marcel for your friendship. Sandro, my dear friend and brother, the river is waiting for us.

Thanks to my parents who taught me the important things. Thanks to my siblings for sharing the good and tough moments. Thanks Jenni for your help with the Ãě.

Ana, thank you so much for filling the air with a true mix of peace, positive energy — and curiosity.

References

Albert, R., Jeong, H., Barabasi, A. L., 1999. Internet – diameter of the world-wide web. Nature 401 (6749), 130–131.

Albin, R. L., Young, A. B., Penney, J. B., 1989. The functional anatomy of basal ganglia disorders. Trends in Neurosciences 12 (10), 366–375.

Aldridge, J. W., Berridge, K. C., 1998. Coding of serial order by neostriatal neurons: A "natural action" approach to movement sequence 18 (7), 2777–2787.

Alexander, G. E., Crutcher, M. D., 1990. Functional architecture of basal ganglia circuits: neural substrates of parallel processing. Trends in Neurosciences 13 (7), 266–271.

Amitai, Y., Gibson, J., Beierlein, M., Patrick, S., Ho, A., Connors, B., Golomb, D., 2002. The spatial dimensions of electrically coupled networks of interneurons in the neocortex. Journal of Neuroscience 22 (10), 4142–4152.

Arieli, A., Sterkin, A., Grinvald, A., Aertsen, A., 1996. Dynamics of ongoing activity: Explanation of the large variability in evoked cortical responses. Science 273 (5283), 1868–1871.

Aron, A. R., Poldrack, R. A., 2006. Cortical and subcortical contributions to stop signal response inhibition: Role of the subthalamic nucleus. Journal of Neuroscience 26 (9), 2424–2433.

Auer, P., Burgsteiner, H., Maass, W., 2008. A learning rule for very simple universal approximators consisting of a single layer of perceptrons. Neural Networks 21 (5), 786–795.

Bak, P., Tang, C., Wiesenfeld, K., 1988. Self-organized criticality. Physical Review A 38 (1), 364–374.

Bar-Gad, I., Havazelet-Heimer, G., Goldberg, J., Ruppin, E., Bergman, H., 2000. Reinforcement-driven dimensionality reduction - a model for information processing in the basal ganglia. Journal of Basic and Clinical Physiology and Pharmacology 11 (4), 305–320.

Bar-Gad, I., Morris, G., Bergman, H., 2003. Information processing, dimensionality reduction and reinforcement learning in the basal ganglia. Progress in Neurobiology 71 (6), 439–473.

Beggs, J. M., Plenz, D., 2003. Neuronal avalanches in neocortical circuits. Journal of Neuroscience 23 (35), 11167–11177.

Beierlein, M., Gibson, J., Connors, B., 2000. A network of electrically coupled interneurons drives synchronized inhibition in neocortex. Nature Neuroscience 3, 904–910.

Berendse, H., Groenewegen, H., 1990. Organization of the thalamostriatal projections in the rat, with special emphasis on the ventral striatum. Journal of Comparative Neurology 299 (2), 187–228.

Bergman, H., Feingold, A., Nini, A., Raz, A., Slovin, H., Abeles, M., Vaadia, E., 1998.

Physiological aspects of information processing in the basal ganglia of normal and parkinsonian primates. Trends in Neurosciences 21 (1), 32–38.

Bergman, H., Wichmann, T., DeLong, M. R., 1990. Reversal of experimental parkinsonism by lesions of the subthalamic nucleus. Science 249 (4975), 1436–1438.

Berke, J., Okatan, M., Skurski, J., Eichenbaum, H., 2004. Oscillatory entrainment of striatal neurons in freely moving rats. Neuron 43 (6), 883–896.

Berke, J. D., 2008. Uncoordinated firing rate changes of striatal fast-spiking interneurons during behavioral task performance. Journal of Neuroscience 28 (40), 10075–10080.

Bertran-Gonzalez, J., Hervé, D., Girault, J.-A., Valjent, E., 2010. What is the degree of segregation between striatonigral and striatopallidal projections? Frontiers in Neuroanatomy 4, 136.

Bevan, M., Booth, P., Eaton, S., Bolam, J., 1998. Selective innervation of neostriatal interneurons by a subclass of neuron in the globus pallidus of the rat. Journal of Neuroscience 18 (22), 9438–9452.

Blackwell, K., Czubayko, U., Plenz, D., 2003. Quantitative estimate of synaptic inputs to striatal neurons during up and down states in vitro. Journal of Neuroscience 23 (27), 9123–9132.

Bolam, J. P., Hanley, J. J., Booth, P. a. C., Bevan, M. D., 2000. Synaptic organisation of the basal ganglia. Journal of Anatomy 196 (4), 527–542.

Bower, J., Beeman, D., 1998. The book of GENESIS: exploring realistic neural models with the GEneral NEural SImulation System. Springer-Verlag New York, NY, USA.

Bracci, E., Centonze, D., Bernardi, G., Calabresi, P., 2003. Voltage-dependent membrane potential oscillations of rat striatal fast-spiking interneurons. Journal of Physiology 549 (1), 121–130.

Brown, P., Oliviero, A., Mazzone, P., Insola, A., Tonali, P., Lazzaro, V. D., 2001. Dopamine dependency of oscillations between subthalamic nucleus and pallidum in parkinson's disease. Journal of Neuroscience 21 (3), 1033–1038.

Calabresi, P., Misgeld, U., Dodt, H., 1987. Intrinsic membrane properties of neostriatal neurons can account for their low level of spontaneous activity. Neuroscience 20 (1), 293–303.

Calabresi, P., Picconi, B., Tozzi, A., Di Filippo, M., 2007. Dopamine-mediated regulation of corticostriatal synaptic plasticity. Trends in Neurosciences 30 (5), 211–219.

Carrillo-Reid, L., Tecuapetla, F., Tapia, D., Hernández-Cruz, A., Galarraga, E., Drucker-Colin, R., Bargas, J., 2008. Encoding network states by striatal cell assemblies. Journal of Neurophysiology 99 (3), 1435–1450.

Chung, Y., Shin, C., Kim, M., Cha, C., 2000. Immunohistochemical study on the distribution of six members of the Kv1 channel subunits in the rat basal ganglia. Brain Research 875, 164–170.

Clarke, C. E., Worth, P., Grosset, D., Stewart, D., 2009. Systematic review of apo-

morphine infusion, levodopa infusion and deep brain stimulation in advanced parkinson's disease. Parkinsonism & Related Disorders 15 (10), 728–741.

Clauset, A., Shalizi, C. R., Newman, M. E. J., 2009. Power-law distributions in empirical data. SIAM Review 51 (4), 661–703.

Cruz, A. V., Mallet, N., Magill, P. J., Brown, P., Averbeck, B. B., 2009. Effects of dopamine depletion on network entropy in the external globus pallidus. Journal of Neurophysiology 102 (2), 1092–1102.

Czubayko, U., Plenz, D., 2002. Fast synaptic transmission between striatal spiny projection neurons. Proceedings of the National Academy of Sciences 99 (24), 15764–15769.

Day, M., Wang, Z., Ding, J., An, X., Ingham, C. A., Shering, A. F., Wokosin, D., Ilijic, E., Sun, Z., Sampson, A. R., Mugnaini, E., Deutch, A. Y., Sesack, S. R., Arbuthnott, G. W., Surmeier, D. J., 2006. Selective elimination of glutamatergic synapses on striatopallidal neurons in parkinson disease models. Nature Neuroscience 9 (2), 251–259.

Dehghani, N., Hatsopoulos, N. G., Parker, R. A., Greger, B., Halgren, E., Cash, S. S., Destexhe, A., 2012. Avalanche analysis from multielectrode ensemble recordings in cat, monkey, and human cerebral cortex during wakefulness and sleep. Frontiers in Fractal Physiology 3 (302).

DeLong, M., Wichmann, T., 2009. Update on models of basal ganglia function and dysfunction. Parkinsonism & Related Disorders 15, Supplement 3, S237–S240.

Deniau, J., Chevalier, G., 1985. Disinhibition as a basic process in the expression of striatal functions. II. the striato-nigral influence on thalamocortical cells of the ventromedial thalamic nucleus. Brain Research 334 (2), 227–233.

Denny-Brown, D., 1962. The Basal Ganglia. Oxford University Press.

Di Filippo, M., Picconi, B., Tantucci, M., Ghiglieri, V., Bagetta, V., Sgobio, C., Tozzi, A., Parnetti, L., Calabresi, P., 2009. Short-term and long-term plasticity at corticostriatal synapses: Implications for learning and memory. Behavioural Brain Research 199 (1), 108–118.

Ding, J., Peterson, J. D., Surmeier, D. J., 2008. Corticostriatal and thalamostriatal synapses have distinctive properties. Journal of Neuroscience 28 (25), 6483–6492.

Dominey, P., Arbib, M., Joseph, J.-P., 1995. A model of corticostriatal plasticity for learning oculomotor associations and sequences. Journal of Cognitive Neuroscience 7 (3), 311–336.

Eeckhout, J., 2009. Gibrat's law for (all) cities: Reply. The American Economic Review 99, 1676–1683.

English, D. F., Ibanez-Sandoval, O., Stark, E., Tecuapetla, F., Buzsáki, G., Deisseroth, K., Tepper, J. M., Koos, T., 2012. GABAergic circuits mediate the reinforcement-related signals of striatal cholinergic interneurons. Nature Neuroscience 15 (1), 123–130.

Féger, J., Crossman, A., 1984. Identification of different subpopulations of neostriatal neurones projecting to globus pallidus or substantia nigra in the monkey: A retrograde fluorescence double-labelling study. Neuroscience Letters 49 (1–2), 7–12.

Flaherty, A. W., Graybiel, A. M., 1994. Input-output organization of the sensorimotor striatum in the squirrel monkey. Journal of Neuroscience 14 (2), 599–610.

Fox, M. D., Raichle, M. E., Sep. 2007. Spontaneous fluctuations in brain activity observed with functional magnetic resonance imaging. Nature Reviews Neuroscience 8 (9), 700–711.

Fox, M. D., Snyder, A. Z., Zacks, J. M., Raichle, M. E., 2005. Coherent spontaneous activity accounts for trial-to-trial variability in human evoked brain responses. Nature Neuroscience 9 (1), 23–25.

Fukuda, T., 2009. Network architecture of gap junction-coupled neuronal linkage in the striatum. Journal of Neuroscience 29 (4), 1235–1243.

Gage, G. J., Stoetzner, C. R., Wiltschko, A. B., Berke, J. D., 2010. Selective activation of striatal fast-spiking interneurons during choice execution. Neuron 67 (3), 466–479.

Gähwiler, B. H., Thompson, S. M., Muller, D., 2001. Preparation and maintenance of organotypic slice cultures of CNS tissue. In: Crawley, J. N., Gerfen, C. R., Rogawski, M. A., Sibley, D. R., Skolnick, P., Wray, S. (Eds.), Current Protocols in Neuroscience. John Wiley & Sons, Inc., Hoboken, NJ, USA.

Galarreta, M., Hestrin, S., 1999. A network of fast-spiking cells in the neocortex connected by electrical synapses. Nature 402 (6757), 72–75.

Galarreta, M., Hestrin, S., 2001. Electrical synapses between GABA-releasing interneurons. Nature Reviews Neuroscience 2 (6), 425–433.

Galarreta, M., Hestrin, S., 2002. Electrical and chemical synapses among parvalbumin fast-spiking GABAergic interneurons in adult mouse neocortex. Proceedings of the National Academy of Sciences 99 (19), 12438–12443.

Gerfen, C. R., 1989. The neostriatal mosaic: striatal patch-matrix organization is related to cortical lamination. Science 246 (4928), 385–388.

Gerfen, C. R., Engber, T. M., Mahan, L. C., Susel, Z., Chase, T. N., Monsma, F J, J., Sibley, D. R., 1990. D1 and d2 dopamine receptor-regulated gene expression of striatonigral and striatopallidal neurons. Science 250 (4986), 1429–1432.

Gerfen, C. R., Sawchenko, P. E., 1984. An anterograde neuroanatomical tracing method that shows the detailed morphology of neurons, their axons and terminals: immunohistochemical localization of an axonally transported plant lectin, phaseolus vulgaris leucoagglutinin (PHA-L). Brain research 290 (2), 219–238.

Gerfen, C. R., Surmeier, D. J., 2011. Modulation of striatal projection systems by dopamine. Annual Review of Neuroscience 34 (1), 441–466.

Gireesh, E. D., Plenz, D., 2008. Neuronal avalanches organize as nested theta- and beta/gamma-oscillations during development of cortical layer 2/3. Proceedings

of the National Academy of Sciences 105 (21), 7576–7581.

Gibson, J. R., Beierlein, M., Connors, B. W., 2005. Functional properties of electrical synapses between inhibitory interneurons of neocortical layer 4. Journal of Neurophysiology 93 (1), 467–480.

Gillies, A., Arbuthnott, G., 2000. Computational models of the basal ganglia. Movement Disorders 15 (5), 762–770.

Gittis, A., Hang, G., LaDow, E., Shoenfeld, L., Atallah, B., Finkbeiner, S., Kreitzer, A., 2011. Rapid target-specific remodeling of fast-spiking inhibitory circuits after loss of dopamine. Neuron 71 (5), 858–868.

Gittis, A. H., Nelson, A. B., Thwin, M. T., Palop, J. J., Kreitzer, A. C., 2010. Distinct roles of GABAergic interneurons in the regulation of striatal output pathways. Journal of Neuroscience 30 (6), 2223–2234.

Goldberg, E., Clark, B., Zagha, E., Nahmani, M., Erisir, A., B, R., 2008. K^+ channels at the axon initial segment dampen near-threshold excitability of neocortical fast-spiking GABAergic interneurons. Neuron 58 (3), 387–400.

Goldberg, J., Reynolds, J., 2011. Spontaneous firing and evoked pauses in the tonically active cholinergic interneurons of the striatum. Neuroscience 198, 27–43.

Goldberg, J. A., Wilson, C. J., 2010. The cholinergic interneurons of the striatum: intrinsic properties underlie multiple discharge patterns. In: Steiner, H., Tseng, K. Y. (Eds.), Handbook of basal ganglia structure and function. pp. 133–149.

Goldstein, M. L., Morris, S. A., Yen, G. G., 2004. Problems with fitting to the power-law distribution. European Physical Journal B 41 (4), 255–258.

Golomb, D., Donner, K., Shacham, L., Shlosberg, D., Amitai, Y., Hansel, D., 2007. Mechanisms of firing patterns in fast-spiking cortical interneurons. PLoS Computational Biology 3 (8), e156.

Gradinaru, V., Mogri, M., Thompson, K. R., Henderson, J. M., Deisseroth, K., 2009. Optical deconstruction of parkinsonian neural circuitry. Science 324 (5925), 354–359.

Graybiel, A. M., 2008. Habits, rituals, and the evaluative brain. Annual Review of Neuroscience 31 (1), 359–387.

Grewe, B. F., Langer, D., Kasper, H., Kampa, B. M., Helmchen, F., 2010. High-speed in vivo calcium imaging reveals neuronal network activity with near-millisecond precision. Nature Methods 7 (5), 399–405.

Gustafson, N., Gireesh-Dharmaraj, E., Czubayko, U., Blackwell, K. T., Plenz, D., 2006. A comparative voltage and current-clamp analysis of feedback and feedforward synaptic transmission in the striatal microcircuit in vitro. Journal of Neurophysiology 95 (2), 737–752.

Guzmán, J. N., Hernández, A., Galarraga, E., Tapia, D., Laville, A., Vergara, R., Aceves, J., Bargas, J., 2003. Dopaminergic modulation of axon collaterals interconnecting spiny neurons of the rat striatum. Journal of Neuroscience 23 (26), 8931–8940.

Haber, S. N., Calzavara, R., 2009. The cortico-basal ganglia integrative network: The role of the thalamus. Brain Research Bulletin 78 (2-3), 69–74.

Hahn, G., Petermann, T., Havenith, M. N., Yu, S., Singer, W., Plenz, D., Nikolić, D., 2010. Neuronal avalanches in spontaneous activity in vivo. Journal of Neurophysiology 104 (6), 3312–3322.

Hald, A., 1999. On the history of maximum likelihood in relation to inverse probability and least squares. Statistical Science 14 (2), 214–222.

Hammond, C., Bergman, H., Brown, P., 2007. Pathological synchronization in parkinson's disease: networks, models and treatments. Trends in Neurosciences 30 (7), 357–364.

Harris, K. D., Thiele, A., 2011. Cortical state and attention. Nature Reviews Neuroscience 12 (9), 509–523.

Hjorth, J., Blackwell, K., Hellgren Kotaleski, J., 2009. Gap junctions between striatal fast-spiking interneurons regulate spiking activity and synchronisation as a function of cortical activity. Journal of Neuroscience 29 (16), 5276–5286.

Hobbs, J. P., Smith, J. L., Beggs, J. M., 2010. Aberrant neuronal avalanches in cortical tissue removed from juvenile epilepsy patients. Journal of Clinical Neurophysiology 27 (6), 380–386.

Hornik, K., Stinchcombe, M., White, H., 1989. Multilayer feedforward networks are universal approximators. Neural Networks 2 (5), 359–366.

Humphries, M. D., Wood, R., Gurney, K., 2009. Dopamine-modulated dynamic cell assemblies generated by the GABAergic striatal microcircuit. Neural Networks 22 (8), 1174–1188.

Ibáñez Sandoval, O., Tecuapetla, F., Unal, B., Shah, F., Koós, T., Tepper, J. M., 2011. A novel functionally distinct subtype of striatal neuropeptide Y interneuron. Journal of Neuroscience 31 (46), 16757–16769.

Ikegaya, Y., Bon-Jego, M. L., Yuste, R., 2005. Large-scale imaging of cortical network activity with calcium indicators. Neuroscience Research 52 (2), 132–138.

Jaeger, D., Kita, H., Wilson, C., 1994. Surround inhibition among projection neurons is weak or nonexistent in the rat neostriatum. Journal of Neurophysiology 72 (5), 2555–2558.

Jensen, H. J., 1998. Self-organized criticality: emergent complex behavior in physical and biological systems. Cambridge University Press, Cambridge, United Kingdom.

Jones, E. G., Leavitt, R. Y., 1974. Retrograde axonal transport and the demonstration of non-specific projections to the cerebral cortex and striatum from thalamic intralaminar nuclei in the rat, cat and monkey. Journal of Comparative Neurology 154 (4), 349–377.

Jones, J. H., Handcock, M. S., 2003. An assessment of preferential attachment as a mechanism for human sexual network formation. Proceedings of the Royal Society of London. Series B: Biological Sciences 270 (1520), 1123 –1128.

Joshua, M., Adler, A., Mitelman, R., Vaadia, E., Bergman, H., 2008. Midbrain dopaminergic neurons and striatal cholinergic interneurons encode the difference between reward and aversive events at different epochs of probabilistic classical conditioning trials. Journal of Neuroscience 28 (45), 11673–11684.

Kalanithi, P. S. A., Zheng, W., Kataoka, Y., DiFiglia, M., Grantz, H., Saper, C. B., Schwartz, M. L., Leckman, J. F., Vaccarino, F. M., 2005. Altered parvalbumin-positive neuron distribution in basal ganglia of individuals with tourette syndrome. Proceedings of the National Academy of Sciences of the United States of America 102 (37), 13307–13312.

Katayama, Y., Miyazaki, S., Tsubokawa, T., 1981. Electrophysiological evidence favoring intracaudate axon collaterals of GABAergic caudate output neurons in the cat. Brain Research 216 (1), 180–186.

Kawaguchi, Y., Kubota, Y., 1997. GABAergic cell subtypes and their synaptic connections in rat frontal cortex. Cerebral Cortex 7 (6), 476–486.

Kawaguchi, Y., Wilson, C. J., Augood, S. J., Emson, P. C., 1995. Striatal interneurones: chemical, physiological and morphological characterization. Trends in Neurosciences 18 (12), 527–535.

Kawaguchi, Y., 1993. Physiological, morphological, and histochemical characterization of three classes of interneurons in rat neostriatum. Journal of Neuroscience 13 (11), 4908–4923.

Kawaguchi, Y., 1997. Neostriatal cell subtypes and their functional roles. Neuroscience Research 27 (1), 1–8.

Kemp, J., Powell, T., 1970. The cortico-striate projection in the monkey. Brain 93 (3), 525–46.

Kermadi, I., Joseph, J. P., 1995. Activity in the caudate nucleus of monkey during spatial sequencing. Journal of Neurophysiology 74 (3), 911–933.

Kerr, J. N. D., Plenz, D., 2004. Action potential timing determines dendritic calcium during striatal up-states. Journal of Neuroscience 24 (4), 877–885.

Kincaid, A. E., Zheng, T., Wilson, C. J., 1998. Connectivity and convergence of single corticostriatal axons. Journal of Neuroscience 18 (12), 4722–4731.

Kinouchi, O., Copelli, M., 2006. Optimal dynamical range of excitable networks at criticality. Nature Physics 2 (5), 348–351.

Kita, H., Kosaka, T., Heizmann, C., 1990. Parvalbumin-immunoreactive neurons in the rat neostriatum: A light and electron microscopic study. Brain research 536 (1-2), 1–15.

Klaus, A., Yu, S., Plenz, D., 2011. Statistical analyses support power law distributions found in neuronal avalanches. PLoS ONE 6 (5), e19779.

Klostermann, O., Wahle, P., 1999. Patterns of spontaneous activity and morphology of interneuron types in organotypic cortex and thalamus-cortex cultures. Neuroscience 92 (4), 1243–1259.

Koós, T., Tepper, J., Wilson, C., 2004. Comparison of IPSCs evoked by spiny and fast-spiking neurons in the neostriatum. Journal of Neuroscience 24 (36), 7916–7922.

Koós, T., Tepper, J. M., 1999. Inhibitory control of neostriatal projection neurons by GABAergic interneurons. Nature Neuroscience 2 (5), 467–472.

Koós, T., Tepper, J. M., 2002. Dual cholinergic control of fast-spiking interneurons in the neostriatum. Journal of Neuroscience 22 (2), 529–535.

Kotaleski, J., Plenz, D., Blackwell, K., 2006. Using potassium currents to solve signal-to-noise problems in inhibitory feedforward networks of the striatum. Journal of Neurophysiology 95 (1), 331–341.

Kovalchuk, Y., Eilers, J., Lisman, J., Konnerth, A., 2000. NMDA receptor-mediated subthreshold Ca^{2+} signals in spines of hippocampal neurons. Journal of Neuroscience 20 (5), 1791–1799.

Kreitzer, A. C., Malenka, R. C., 2007. Endocannabinoid-mediated rescue of striatal LTD and motor deficits in parkinson's disease models. Nature 445 (7128), 643–647.

La Camera, G., Rauch, A., Thurbon, D., Lüscher, H., Senn, W., Fusi, S., 2006. Multiple time scales of temporal response in pyramidal and fast spiking cortical neurons. Journal of Neurophysiology 96 (6), 3448–3464.

Lapper, S., Bolam, J., 1992. Input from the frontal cortex and the parafascicular nucleus to cholinergic interneurons in the dorsal striatum of the rat. Neuroscience 51 (3), 533–545.

Lapper, S., Smith, Y., Sadikot, A., Parent, A., Bolam, J., 1992. Cortical input to parvalbumin-immunoreactive neurones in the putamen of the squirrel monkey. Brain Research 580 (1–2), 215–224.

Leblois, A., Boraud, T., Meissner, W., Bergman, H., Hansel, D., 2006. Competition between feedback loops underlies normal and pathological dynamics in the basal ganglia. Journal of Neuroscience 26 (13), 3567–3583.

Lenz, S., Perney, T., Qin, Y., Robbins, E., Chesselet, M., 1994. GABAergic interneurons of the striatum express the shaw-like potassium channel Kv3.1. Synapse 18 (1), 55–66.

Levy, M., 2009. Gibrat's law for (all) cities: Comment. The American Economic Review 99, 1672–1675.

Liljeros, F., Edling, C. R., Amaral, L. A. N., Stanley, H. E., Aberg, Y., 2001. The web of human sexual contacts. Nature 411 (6840), 907–908.

Lovinger, D. M., 2010. Neurotransmitter roles in synaptic modulation, plasticity and learning in the dorsal striatum. Neuropharmacology 58 (7), 951–961.

Luk, K. C., Sadikot, A. F., 2001. GABA promotes survival but not proliferation of parvalbumin-immunoreactive interneurons in rodent neostriatum: an in vivo study with stereology. Neuroscience 104 (1), 93–103.

Magazanik, L. G., Buldakova, S. L., Samoilova, M. V., Gmiro, V. E., Mellor, I. R.,

Usherwood, P. N. R., 1997. Block of open channels of recombinant AMPA receptors and native AMPA/kainate receptors by adamantane derivatives. Journal of Physiology 505 (3), 655–663.

Mahon, S., Delord, B., Deniau, J.-M., Charpier, S., 2000. Intrinsic properties of rat striatal output neurones and time-dependent facilitation of cortical inputs in vivo. Journal of Physiology 527 (2), 345–354.

Mainen, Z., Sejnowski, T., 1995. Reliability of spike timing in neocortical neurons. Science 268 (5216), 1503–1506.

Malevergne, Y., Pisarenko, V., Sornette, D., 2009. Gibrat's law for cities: uniformly most powerful unbiased test of the Pareto against the lognormal. arXiv:0909.1281.

Mallet, N., Micklem, B., Henny, P., Brown, M., Williams, C., Bolam, J., Nakamura, K., Magill, P., 2012. Dichotomous organization of the external globus pallidus. Neuron 74 (6), 1075–1086.

Mancilla, J., Lewis, T., Pinto, D., Rinzel, J., Connors, B., 2007. Synchronization of electrically coupled pairs of inhibitory interneurons in neocortex. Journal of Neuroscience 27 (8), 2058.

Marín, O., Anderson, S. A., Rubenstein, J. L. R., 2000. Origin and molecular specification of striatal interneurons. Journal of Neuroscience 20 (16), 6063–6076.

Markram, H., Wang, Y., Tsodyks, M., 1998. Differential signaling via the same axon of neocortical pyramidal neurons. Proceedings of the National Academy of Sciences 95 (9), 5323–5328.

Markram, H., Toledo-Rodriguez, M., Wang, Y., Gupta, A., Silberberg, G., Wu, C., 2004. Interneurons of the neocortical inhibitory system. Nature Reviews Neuroscience 5 (10), 793–807.

Marsden, C. D., Obeso, J. A., 1994. The functions of the basal ganglia and the paradox of stereotaxic surgery in parkinson's disease. Brain 117 (4), 877–897.

Mattis, J., Tye, K. M., Ferenczi, E. A., Ramakrishnan, C., O'Shea, D. J., Prakash, R., Gunaydin, L. A., Hyun, M., Fenno, L. E., Gradinaru, V., Yizhar, O., Deisseroth, K., 2012. Principles for applying optogenetic tools derived from direct comparative analysis of microbial opsins. Nature Methods 9 (2), 159–172.

McCairn, K. W., Bronfeld, M., Belelovsky, K., Bar-Gad, I., 2009. The neurophysiological correlates of motor tics following focal striatal disinhibition. Brain 132 (8), 2125–2138.

McFarland, N. R., Haber, S. N., 2000. Convergent inputs from thalamic motor nuclei and frontal cortical areas to the dorsal striatum in the primate. Journal of Neuroscience 20 (10), 3798–3813.

McGeorge, A., Faull, R., 1989. The organization of the projection from the cerebral cortex to the striatum in the rat. Neuroscience 29 (3), 503–537.

Meisel, C., Storch, A., Hallmeyer-Elgner, S., Bullmore, E., Gross, T., 2012. Failure of adaptive self-organized criticality during epileptic seizure attacks. PLoS Comput

Biol 8 (1), e1002312.

Miller, B. R., Walker, A. G., Shah, A. S., Barton, S. J., Rebec, G. V., 2008. Dysregulated information processing by medium spiny neurons in striatum of freely behaving mouse models of huntington's disease. Journal of Neurophysiology 100 (4), 2205–2216.

Mitzenmacher, M., 2004. A brief history of generative models for power law and lognormal distributions. Internet Mathematics 1 (2), 226–251.

Morris, G., Arkadir, D., Nevet, A., Vaadia, E., Bergman, H., 2004. Coincident but distinct messages of midbrain dopamine and striatal tonically active neurons. Neuron 43 (1), 133–143.

Muramatsu, S., Yoshida, M., Nakamura, S., 1990. Electrophysiological study of dyskinesia produced by microinjection of picrotoxin into the striatum of the rat. Neuroscience Research 7 (4), 369–380.

Nambu, A., 2008. Seven problems on the basal ganglia. Current Opinion in Neurobiology 18 (6), 595–604.

Newman, M. E. J., 2005. Power laws, pareto distributions and Zipf's law. Contemporary Physics 46 (5), 323–351.

Nini, A., Feingold, A., Slovin, H., Bergman, H., 1995. Neurons in the globus pallidus do not show correlated activity in the normal monkey, but phase-locked oscillations appear in the MPTP model of parkinsonism. Journal of Neurophysiology 74 (4), 1800–1805.

Nisenbaum, E. S., Wilson, C. J., 1995. Potassium currents responsible for inward and outward rectification in rat neostriatal spiny projection neurons. Journal of Neuroscience 15 (6), 4449–4463.

Nomura, M., Fukai, T., Aoyagi, T., 2003. Synchrony of Fast-Spiking interneurons interconnected by GABAergic and electrical synapses. Neural Computation 15 (9), 2179–2198.

Oorschot, D. E., 1996. Total number of neurons in the neostriatal, pallidal, subthalamic, and substantia nigral nuclei of the rat basal ganglia: A stereological study using the cavalieri and optical disector methods. Journal of Comparative Neurology 366, 580–599.

Parent, A., Hazrati, L. N., 1995. Functional anatomy of the basal ganglia. i. the cortico-basal ganglia-thalamo-cortical loop. Brain research. Brain research reviews 20 (1), 91–127.

Parent, A., Sato, F., Wu, Y., Gauthier, J., Lévesque, M., Parent, M., 2000. Organization of the basal ganglia: the importance of axonal collateralization. Trends in Neurosciences 23, Supplement 1 (10), S20–S27.

Park, M. R., Lighthall, J. W., Kitai, S. T., 1980. Recurrent inhibition in the rat neostriatum. Brain Research 194 (2), 359–369.

Pasquale, V., Massobrio, P., Bologna, L., Chiappalone, M., Martinoia, S., 2008. Self-organization and neuronal avalanches in networks of dissociated cortical neurons.

Neuroscience 153 (4), 1354–1369.

Pawitan, Y., 2001. In all likelihood: statistical modelling and inference using likelihood. Oxford University Press, New York, USA.

Perez-Rosello, T., Figueroa, A., Salgado, H., Vilchis, C., Tecuapetla, F., Guzman, J. N., Galarraga, E., Bargas, J., 2005. Cholinergic control of firing pattern and neurotransmission in rat neostriatal projection neurons: role of CaV2.1 and CaV2.2 Ca^{2+} channels. Journal of Neurophysiology 93 (5), 2507–2519.

Petermann, T., Thiagarajan, T. C., Lebedev, M. A., Nicolelis, M. A. L., Chialvo, D. R., Plenz, D., 2009. Spontaneous cortical activity in awake monkeys composed of neuronal avalanches. Proceedings of the National Academy of Sciences 106 (37), 15921–15926.

Planert, H., Szydlowski, S. N., Hjorth, J. J. J., Grillner, S., Silberberg, G., 2010. Dynamics of synaptic transmission between fast-spiking interneurons and striatal projection neurons of the direct and indirect pathways. Journal of Neuroscience 30 (9), 3499–3507.

Plenz, D., 2003. When inhibition goes incognito: feedback interaction between spiny projection neurons in striatal function. Trends in Neurosciences 26 (8), 436–443.

Plenz, D., 2012. Neuronal avalanches and coherence potentials. The European Physical Journal - Special Topics 205 (1), 259–301.

Plenz, D., Aertsen, A., 1996a. Neural dynamics in cortex-striatum co-cultures–I. Anatomy and electrophysiology of neuronal cell types. Neuroscience 70 (4), 861–891.

Plenz, D., Aertsen, A., 1996b. Neural dynamics in cortex-striatum co-cultures–II. Spatiotemporal characteristics of neuronal activity. Neuroscience 70 (4), 893–924.

Plenz, D., Kitai, S. T., 1998a. Up and down states in striatal medium spiny neurons simultaneously recorded with spontaneous activity in fast-spiking interneurons studied in cortex-striatum-substantia nigra organotypic cultures. Journal of Neuroscience 18 (1), 266–283.

Plenz, D., Kitai, S. T., 1998b. Regulation of the nigrostriatal pathway by metabotropic glutamate receptors during development. Journal of Neuroscience 18 (11), 4133–4144.

Plenz, D., Kitai, S. T., 2000. Adaptive classification of cortical input to the striatum by competitive learning. In: Miller, R., Wickens, J. R. (Eds.), Brain Dynamics and The Striatal Complex. CRC Press, pp. 165–177.

Plenz, D., Kital, S. T., 1999. A basal ganglia pacemaker formed by the subthalamic nucleus and external globus pallidus. Nature 400 (6745), 677–682.

Plenz, D., Stewart, C. V., Shew, W., Yang, H., Klaus, A., Bellay, T., 2011. Multi-electrode array recordings of neuronal avalanches in organotypic cultures. Journal of Visualized Experiments (54).

Ponzi, A., Wickens, J., 2010. Sequentially switching cell assemblies in random in-

hibitory networks of spiking neurons in the striatum. Journal of Neuroscience 30 (17), 5894–5911.

Powell, T. P. S., Cowan, W. M., 1956. A study of thalamo-striate relations in the monkey. Brain 79 (2), 364–366.

Press, W. H., Teukolsky, S. A., Vetterling, W. T., Flannery, B. P., 2007. Numerical Recipes: The Art of Scientific Computing. Cambridge University Press, New York, USA.

Rabinovich, M., Huerta, R., Volkovskii, A., Abarbanel, H., Stopfer, M., Laurent, G., 2000. Dynamical coding of sensory information with competitive networks. Journal of Physiology (Paris) 94 (5–6), 465–471.

Ramanathan, S., Hanley, J., Deniau, J., Bolam, J., 2002. Synaptic convergence of motor and somatosensory cortical afferents onto GABAergic interneurons in the rat striatum. Journal of Neuroscience 22 (18), 8158.

Raz, A., Feingold, A., Zelanskaya, V., Vaadia, E., Bergman, H., 1996. Neuronal synchronization of tonically active neurons in the striatum of normal and parkinsonian primates. Journal of Neurophysiology 76 (3), 2083–2088.

Redgrave, P., Rodriguez, M., Smith, Y., Rodriguez-Oroz, M. C., Lehericy, S., Bergman, H., Agid, Y., DeLong, M. R., Obeso, J. A., 2010. Goal-directed and habitual control in the basal ganglia: implications for parkinson's disease. Nature Reviews Neuroscience 11 (11), 760–772.

Reig, R., Gallego, R., Nowak, L. G., Sanchez-Vives, M. V., 2006. Impact of cortical network activity on short-term synaptic depression. Cerebral Cortex 16 (5), 688–695.

Reig, R., Sanchez-Vives, M. V., 2007. Synaptic transmission and plasticity in an active cortical network. PLoS ONE 2 (8), e670.

Reig, R., Silberberg, G., 2012. Bilateral and multisensory integration in striatal microcircuits. Program No. 380.11. 2012 Neuroscience Meeting Planner. New Orleans, LA: Society for Neuroscience, 2012. Online.

Reynolds, J. N. J., Hyland, B. I., Wickens, J. R., 2001. A cellular mechanism of reward-related learning. Nature 413 (6851), 67–70.

Ribeiro, T. L., Copelli, M., Caixeta, F., Belchior, H., Chialvo, D. R., Nicolelis, M. A. L., Ribeiro, S., 2010. Spike avalanches exhibit universal dynamics across the sleep-wake cycle. PLoS ONE 5 (11), e14129.

Ringach, D. L., 2009. Spontaneous and driven cortical activity: implications for computation. Current Opinion in Neurobiology 19 (4), 439–444.

Schneidman, E., Freedman, B., Segev, I., 1998. Ion channel stochasticity may be critical in determining the reliability and precision of spike timing. Neural Computation 10 (70), 1679–1703.

Selemon, L. D., Goldman-Rakic, P. S., 1985. Longitudinal topography and interdigitation of corticostriatal projections in the rhesus monkey. Journal of Neuroscience 5 (3), 776–794.

Shew, W. L., Yang, H., Petermann, T., Roy, R., Plenz, D., 2009. Neuronal avalanches imply maximum dynamic range in cortical networks at criticality. Journal of Neuroscience 29 (49), 15595–15600.

Shew, W. L., Yang, H., Yu, S., Roy, R., Plenz, D., 2011. Information capacity and transmission are maximized in balanced cortical networks with neuronal avalanches. Journal of Neuroscience 31 (1), 55–63.

Shriki, O., Alstott, J., Carver, F., Holroyd, T., Henson, R., Smith, M., Coppola, R., Bullmore, E., Plenz, D., 2013. Neuronal avalanches in the resting MEG of the human brain, manuscript under revision.

Smith, M. A., Kohn, A., 2008. Spatial and temporal scales of neuronal correlation in primary visual cortex. Journal of Neuroscience 28 (48), 12591–12603.

Smith, Y., Raju, D., Nanda, B., Pare, J.-F., Galvan, A., Wichmann, T., 2009. The thalamostriatal systems: anatomical and functional organization in normal and parkinsonian states. Brain Research Bulletin 78 (2-3), 60–68.

Smith, Y., Raju, D. V., Pare, J.-F., Sidibe, M., 2004. The thalamostriatal system: a highly specific network of the basal ganglia circuitry. Trends in Neurosciences 27 (9), 520–527.

Soubrié, P., Reisine, T., Glowinski, J., 1984. Functional aspects of serotonin transmission in the basal ganglia: A review and in vivo approach using the push-pull cannula technique. Neuroscience 13 (3), 605–625.

Standefer, M. J., Dill, R. E., 1977. The role of GABA in dyskinesias induced by chemical stimulation of the striatum. Life Sciences 21 (10), 1515–1519.

Stern, E. A., Jaeger, D., Wilson, C. J., 1998. Membrane potential synchrony of simultaneously recorded striatal spiny neurons in vivo. Nature 394 (6692), 475–478.

Stern, E. A., Kincaid, A. E., Wilson, C. J., 1997. Spontaneous subthreshold membrane potential fluctuations and action potential variability of rat corticostriatal and striatal neurons in vivo. Journal of Neurophysiology 77 (4), 1697–1715.

Stewart, C. V., Plenz, D., 2006. Inverted-U profile of dopamine-NMDA-mediated spontaneous avalanche recurrence in superficial layers of rat prefrontal cortex. Journal of Neuroscience 26 (31), 8148–8159.

Stoppini, L., Buchs, P.-A., Muller, D., 1991. A simple method for organotypic cultures of nervous tissue. Journal of Neuroscience Methods 37 (2), 173–182.

Szydlowski, S. N., Pollak Dorocic, I., Planert, H., Carlén, M., Meletis, K., Silberberg, G., 2013. Target selectivity of feedforward inhibition by striatal fast-spiking interneurons, in press.

Tagliazucchi, E., Balenzuela, P., Fraiman, D., Chialvo, D. R., 2012. Criticality in large-scale brain fMRI dynamics unveiled by a novel point process analysis. Frontiers in Fractal Physiology 3, 15.

Tanaka, T., Kaneko, T., Aoyagi, T., 2008. Recurrent infomax generates cell assemblies, neuronal avalanches, and simple cell-like selectivity. Neural Computation 21 (4), 1038–1067.

Taverna, S., Canciani, B., Pennartz, C., 2007. Membrane properties and synaptic connectivity of fast-spiking interneurons in rat ventral striatum. Brain Research 1152, 49–56.

Taverna, S., Ilijic, E., Surmeier, D. J., 2008. Recurrent collateral connections of striatal medium spiny neurons are disrupted in models of parkinson's disease. Journal of Neuroscience 28 (21), 5504–5512.

Taverna, S., van Dongen, Y., Groenewegen, H., Pennartz, C., 2004. Direct physiological evidence for synaptic connectivity between medium-sized spiny neurons in rat nucleus accumbens in situ. Journal of Neurophysiology 91 (3), 1111–1121.

Tecuapetla, F., Carrillo-Reid, L., Bargas, J., Galarraga, E., 2007. Dopaminergic modulation of short-term synaptic plasticity at striatal inhibitory synapses. Proceedings of the National Academy of Sciences 104 (24), 10258–10263.

Tepper, J., Koós, T., Wilson, C., 2004. GABAergic microcircuits in the neostriatum. Trends in Neurosciences 27 (11), 662–669.

Tepper, J. M., Tecuapetla, F., Ibáñez Sandoval, O., 2010. Heterogeneity and diversity of striatal GABAergic interneurons. Frontiers in Neuroanatomy 4, 150.

Tritsch, N., Sabatini, B., 2012. Dopaminergic modulation of synaptic transmission in cortex and striatum. Neuron 76 (1), 33–50.

Tritsch, N. X., Ding, J. B., Sabatini, B. L., 2012. Dopaminergic neurons inhibit striatal output through non-canonical release of GABA. Nature 490 (7419), 262–266.

Tseng, K. Y., Kasanetz, F., Kargieman, L., Riquelme, L. A., Murer, M. G., 2001. Cortical slow oscillatory activity is reflected in the membrane potential and spike trains of striatal neurons in rats with chronic nigrostriatal lesions. Journal of Neuroscience 21 (16), 6430–6439.

Tsodyks, M., Pawelzik, K., Markram, H., 1998. Neural networks with dynamic synapses. Neural Computation 10 (4), 821–835.

Tunstall, M. J., Oorschot, D. E., Kean, A., Wickens, J. R., 2002. Inhibitory interactions between spiny projection neurons in the rat striatum. Journal of Neurophysiology 88 (3), 1263–1269.

Vonsattel, J. P., DiFiglia, M., 1998. Huntington disease. Journal of Neuropathology and Experimental Neurology 57 (5), 369–384.

Weiser, M., Vega-Saenz de Miera, E., Kentros, C., Moreno, H., Franzen, L., Hillman, D., Baker, H., B, R., 1994. Differential expression of shaw-related K^+ channels in the rat central nervous system. Journal of Neuroscience 14 (3), 949–972.

Wichmann, T., DeLong, M. R., 1996. Functional and pathophysiological models of the basal ganglia. Current Opinion in Neurobiology 6 (6), 751–758.

Wickens, J., Arbuthnott, G., 1993. The corticostriatal system on computer simulation: an intermediate mechanism for sequencing of actions. In: Arbuthnott, G., Emson, P. (Eds.), Progress in Brain Research. Vol. 99. Elsevier, pp. 325–339.

Wickens, J. R., Alexander, M. E., Miller, R., 1991. Two dynamic modes of striatal

function under dopaminergic-cholinergic control: Simulation and analysis of a model. Synapse 8 (1), 1–12.

Wickens, J. R., Oorschot, D. E., 2000. Neural dynamics and surround inhibition in the neostriatum: a possible connection. In: Miller, R., Wickens, J. R. (Eds.), Brain Dynamics and The Striatal Complex. CRC Press, pp. 141–150.

Wilson, C., 2004. In: Shepherd, G. (Ed.), The synaptic organization of the brain, 5th Edition. Oxford University Press New York, Ch. 9. Basal Ganglia, pp. 361–413.

Wilson, C. J., 2007. GABAergic inhibition in the neostriatum. In: James M. Tepper, E. D. A., Bolam, J. P. (Eds.), Progress in Brain Research. Vol. Volume 160. Elsevier, pp. 91–110.

Wilson, C. J., 2009. What controls the timing of striatal spiny cell action potentials in the up state? In: Groenewegen, H. J., Voorn, P., Berendse, H. W., Mulder, A. B., Cools, A. R. (Eds.), The Basal Ganglia IX. No. 58 in Advances in Behavioral Biology. Springer New York, pp. 49–61.

Wilson, C. J., Chang, H. T., Kitai, S. T., 1990. Firing patterns and synaptic potentials of identified giant aspiny interneurons in the rat neostriatum. Journal of Neuroscience 10 (2), 508–519.

Wilson, C. J., Groves, P. M., 1980. Fine structure and synaptic connections of the common spiny neuron of the rat neostriatum: a study employing intracellular injection of horseradish peroxidase. Journal of Comparative Neurology 194 (3), 599–615.

Wilson, C. J., Kawaguchi, Y., 1996. The origins of two-state spontaneous membrane potential fluctuations of neostriatal spiny neurons. Journal of Neuroscience 16 (7), 2397–2410.

Wiltschko, A. B., Pettibone, J. R., Berke, J. D., 2010. Opposite effects of stimulant and antipsychotic drugs on striatal fast-spiking interneurons. Neuropsychopharmacology 35 (6), 1261–1270.

Yang, H., Shew, W. L., Roy, R., Plenz, D., 2012. Maximal variability of phase synchrony in cortical networks with neuronal avalanches. Journal of Neuroscience 32 (3), 1061–1072.

Yin, H. H., Knowlton, B. J., 2006. The role of the basal ganglia in habit formation. Nature Reviews Neuroscience 7 (6), 464–476.

Yu, S., Yang, H., Nakahara, H., Santos, G. S., Nikolić, D., Plenz, D., 2011. Higher-order interactions characterized in cortical activity. Journal of Neuroscience 31 (48), 17514–17526.

Zheng, T., Wilson, C. J., 2002. Corticostriatal combinatorics: The implications of corticostriatal axonal arborizations. Journal of Neurophysiology 87 (2), 1007–1017.

Zhou, F.-M., Liang, Y., Dani, J. A., 2001. Endogenous nicotinic cholinergic activity regulates dopamine release in the striatum. Nature Neuroscience 4 (12), 1224–1229.